CHARACTERIZATION OF THE ACCRETED OPHIOLITE SLICES OF RUTLAND ISLAND, ANDAMAN SEA: EVOLUTION IN A SUPRASUBDUCTION ZONE SETTING

Anindya Bhattacharya*,✉, Tapan Pal** and **Biswajit Ghosh*****

* *Central Petrological Laboratory, Geological Survey of India, Kolkata, India.*
** *Petrology Division, Geological Survey of India, Kolkata, India.*
*** *Department of Geology, University of Calcutta, Kolkata, India.*
✉ *Corresponding author, e-mail: anindya_gsi@rediffmail.com*

Keywords: *Melt-rock interaction, accreted ophiolite slices, suprasubduction zone, boninite. Andaman.*

ABSTRACT

Detailed mapping of 110 km^2 area of the Rutland Island has demarcated four dismembered thrust slices of Cretaceous ophiolite which are interleaved with Eocene sediments. The ophiolite sequence is represented by tectonite, chromitite pods, transitional peridotite, layered ultramafic-mafic, intrusives of plagiogranite-diorite suite and extrusives of basalt and boninite capped by pelagic sediments.

The layered ultramafics and the massive chromitites are characterized by high Mg-olivine (Fo_{92-93}), high Mg-orthopyroxene (En_{88-90}), low CaO (X_{Ca}^{M2} = 0.01 to 0.03), low alumina (Al_2O_3 = 0.66 to 1.20 wt %) and high Cr-chromites, which is typical of boninitic melts in suprasubduction zone (SSZ) environments. The estimated Al_2O_3 contents of the parental melt (10.80 wt%) correspond to a boninitic parental melt. The Type-2 low-Ca boninite extrusives with SiO_2 < 58 wt%, MgO = 8.4 to 9.5 wt% is the extrusive equivalent of boninitic parental lava. As boninitic rocks show higher depletion of Zr and Y than the basaltic rocks, the source rock for boninite was more depleted than that of basalts.

Tectonites showing embayed clinopyroxene grains and irregular shaped Cr-spinel as residual phases preserve records of partial melting. The degree of partial melting of the mantle tectonite has been estimated as ~ 20%, based on Cr content of the spinel. Petrographic features of the transitional peridotites show dissolution of orthopyroxene and clinopyroxene grains and development of small fresh olivine grains along the embayed margins and fractures, displaying melt-rock interaction effects in the mantle rocks. The melt-rock interaction features as well as the bivariant relation of TiO_2 wt% vs. Al_2O_3 wt% of the chromites reflect the evolution of the Rutland ophiolite in a SSZ setting.

INTRODUCTION

Petrological attributes of many of the ophiolites suggest their origin either at suprasubduction zone (SSZ) or ocean ridge environment (Pearce et al., 1984; Stern et al., 1989; Taylor et al., 1992). In SSZ settings the mineralogy and geochemistry of mantle-crustal rocks are influenced by melt-percolation and consequent melt-rock interaction (Kelemen et al., 1990; 1995; McKenzie and O'Nions, 1991; Zhou et al., 1996; 2005; Parkinson and Pearce, 1998; Proenza et al., 1999; Suhr et al., 2003; Zanetti et al., 2006; Piccardo et al., 2007).

The Rutland Island is situated to the south of the South Andaman Islands belongs to an arcuate chain of islands in the central part of the Burma-Andaman-Java subduction complex. The island comprises: 1) thrust-emplaced Cretaceous ophiolite slices and 2) Tertiary sediments. It exposes almost all the major units of an ophiolite, viz. tectonites, transitional peridotite, ultramafic-mafic cumulates, dioritic-plagiogranitic intrusives and extrusives. Geodynamic models and petrological studies of the Andaman ophiolite have been so far carried out in the ophiolite belt exposed in the main Andaman Islands (Pal et al., 2003; Pal, 2011). Ray et al. (1988) and Jafri et al., (1990; 1995) studied the basalt and the plagiogranites of the South Andaman Island. The mineralogical study of the chromites attempted earlier by us, suggested the possible boninitic parentage of the Rutland ophiolite in a SSZ setting (Ghosh et al., 2009).

However, the Rutland Island comprising nearly 40% of the total ophiolite volume exposed in the Andaman and Nicobar Group of Islands has not been studied in detail with respect of field distribution and petrological characterization of the ophiolites. Sheeted dolerite dykes which are very rare in other islands, and the boninitic extrusive equivalent to the estimated boninitic parental melt of the ophiolite, do occur in the Rutland ophiolite sequence. This ophiolite also bears the signature and evidence of melt-rock interaction and other features of SSZ settings. In this paper, new observations from geological mapping and studies on petrological, mineralogical and geochemical aspects of the different lithological units of the Rutland ophiolite will add significant information for understanding the petrogenesis and tectonic setting of the Andaman ophiolite as a whole.

This study involved detailed mapping (1:25,000 scale), petrography, mineral chemistry and bulk chemistry (major and trace element) analyses of the different members of the ophiolite. The distribution of the different thrust slices is shown in the geological map, and the petrological evolution and tectonic setting of the Rutland Ophiolite are discussed here.

GEOLOGICAL SETTING

The Andaman and Nicobar group of islands in the Bay of Bengal form a part of the 5000 km long chain running from Arakan-Yoma in the North to Sumatra and Java in the South (Fig. 1a, b) along which the Indian Plate subducts along the geophysically traced Andaman-Java trench (Curray et al., 1974; Karig et al., 1979; Mukhopadhyay, 1988).

The Andaman Islands expose dismembered slices of Cretaceous ophiolites and Tertiary sediments representing a trench-slope-fore-arc setting. A number of N-S trending dismembered ophiolite slices of Cretaceous age, occurring at

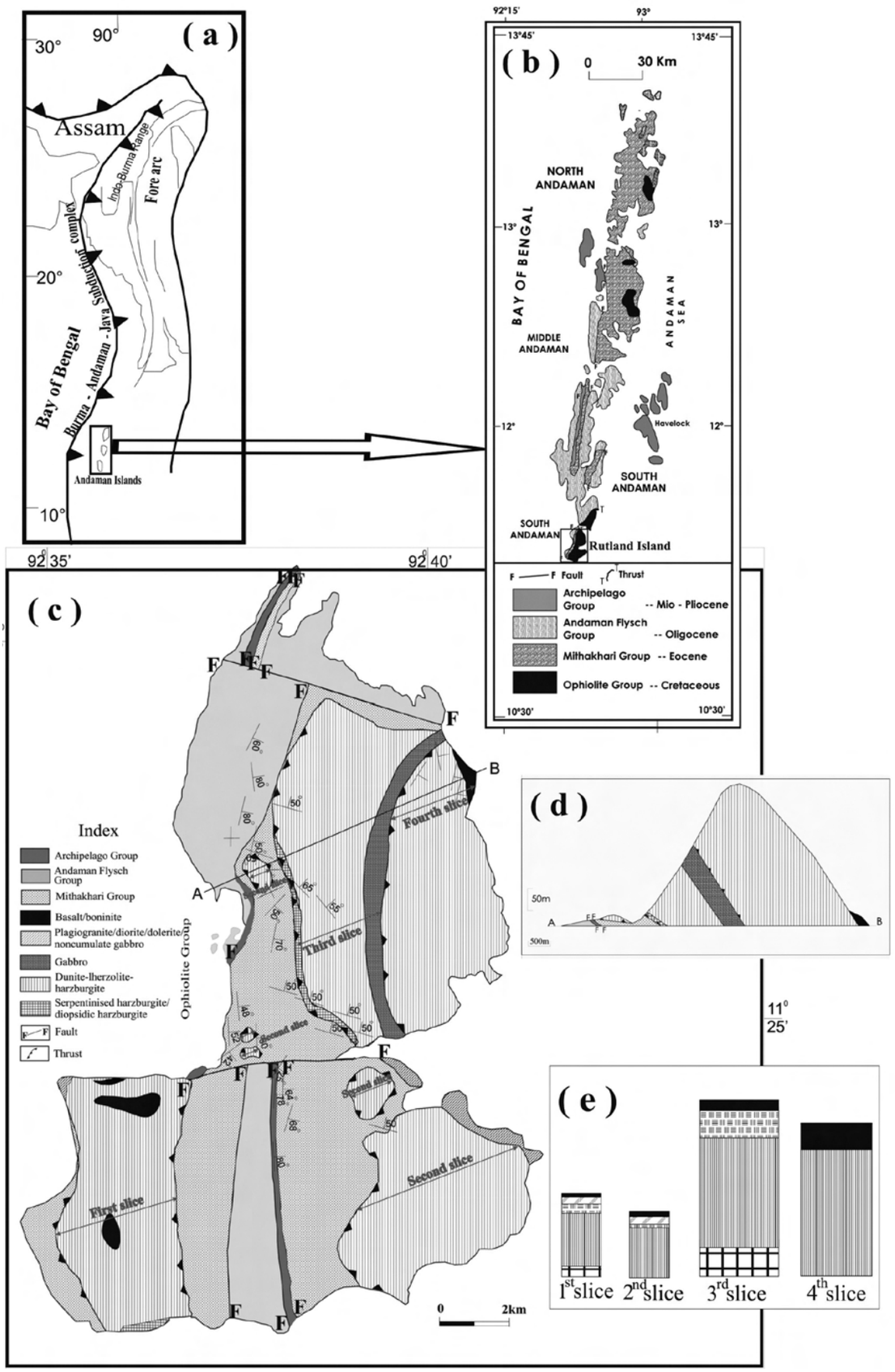

Fig. 1 - a) Regional tectonic elements of the Andaman-Nicobar group of islands in relation to the Java-Burma trench (after Mitchell, 1985); b) location of Rutland Island within the geologic framework of the Andaman group of Islands, with generalized stratigraphy; c) geological map of Rutland Island showing the different ophiolite thrust slices and the different members of the ophiolite, d) geological cross section along line AB on the geological map; e) schematic sequences of the different ophiolite slices.

different structural levels within Eocene trench-slope sediments, were uplifted and emplaced by a series of east-dipping thrusts (Pal et al., 2003). The foraminiferal assemblage of pelagic sediments indicates a Cretaceous age for the Andaman ophiolite (Roy et al., 1988). The Mithakhari Group of sediments of the Andaman Islands contains Eocene fossils (Ray, 1982) and is interpreted a a trench deposit (Chakraborty et al., 1999). The Andaman Flysch Group (stratigraphic age of Late Eocene to Oligocene) represents a turbidite sequence of sandstone-shale with no fossil record, whereas a Mio-Pliocene age is assigned to the Archipelago Group of sediments from the characteristic foraminiferal and nannofossil assemblages (Ray, 1982).

ANALYTICAL TECHNIQUES

X-Ray Fluorescence (XRF): The bulk rock samples representing the different lithologic units of the Rutland ophiolite were analyzed for bulk chemistry. Fresh parts of the samples were crushed and washed thoroughly in water. The crushed and dried rock samples were powdered using a Cup and Ball Mill pulverizer. The finely powdered (-200 mesh) samples were fused into glass discs and analyzed by Wave length dispersive XRF spectrometer (Panalytical Magix 2424 with End window Rh tube) at 30-60 kV and 40-100 mA conditions for bulk major and trace elements. Natural standards supplied by the United States Geological Survey and Centre de Recherches Pétrographiques et Géochimiques (France) were used. Precision and accuracy of the bulk chemical analyses of the different rock types of the Rutland ophiolite, compared with the standard values are given in Appendix 1.

Electron Micro Probe Analysis (EMPA): Polished sections were analyzed with a CAMECA SX100 Electron Probe Micro Analyzer at 15 kV, 12 nA using 1 μm beam diameter for mineral and glass compositions. The natural standards were supplied by BRGM, France (Appendix 2). Results were corrected with a PAP matrix correction program. Fe^{2+} and Fe^{3+} were distributed based on stoichiometry. The standards were analysed at regular intervals to check the precision of sample analysis and 4-8 analytical points were used to calculate the average composition.

LITHOTYPES OF THE RUTLAND OPHIOLITE

The Ophiolite Group of rocks occurs in dismembered slices and consists of the following different members as: a) highly serpentinized and feebly foliated ultramafic sequence at the base, described henceforth as mantle tectonite, b) partly serpentinized harzburgite with apparently massive character, described henceforth as transitional peridotite, c) layered ultramafic-mafic sequence described as cumulate, d) intrusives of dolerite and diorite-plagiogranite compositions and e) extrusives of two types of lava in the form of green lower lava and dark brown to grey upper lava. The pelagic sediments are represented by bedded chert and limestone.

Mantle tectonite

The tectonite unit consists of tectonized and highly serpentinized greenish black ultramafic rocks (lherzolite to harzburgite) showing variably oriented incipient foliation. In the generalized ophiolite stratigraphy it represents the mantle sequence and is also called residual peridotite/tectonite. Locally it contains small pods of dunite, harzburgite and rare chromitite (Fig. 2e).

Petrographically the mantle tectonite unit is represented by highly serpentinized and chloritized lherzolite to harzburgite containing pseudomorphs and relict grains of orthopyroxene, olivine, clinopyroxene and amphibole after pyroxene, where the silicates are dominantly (60-90 vol%) altered. Harzburgites contain 50-70 vol% olivine, 10-40 vol% orthopyroxene, and 2-4 vol% clinopyroxene, 0.5-3.5 vol% chromite. On the other hand lherzolite contains olivine (44-65 vol%), orthopyroxene (23-39 vol%) and clinopyroxene (6-13 vol%).

The pyroxene grains in the tectonite occur both as exsolved and unexsolved (homogenous) grains. Homogenous pyroxene in tectonite is diopside in composition, whereas the exsolved orthopyroxene grains are enstatitic with exsolved lamellae of diopsidic composition (Table 2). Accessory chromites of both lherzolitic and harzburgitic tectonites are anhedral and resorbed with embayed margins (Fig. 3a), and classified as Cr-spinel. Parallel to sub-parallel alignments of orthopyroxene grains and chrome-spinel define the crude foliations. Orthopyroxene grains contain poikilitic inclusions of olivine and chrome-spinel. The olivines within the harzburgite are highly serpentinized and occur as pseudomorphs and relict grains. The serpentine mass shows a mesh, non-pseudomorphic to hourglass textures.

Chromitite pods

The chromitite pods are spheroidal to ellipsoidal in shape ranging from 5 to 25 cm in diameter. A thin serpentinite mass envelopes the chromitite pods. The pods dominantly consist of chromite (~ 90%) with minor serpentine and chlorite. Chromite grains show an overall cumulate texture with adcumulus growth at certain places. Large chromite grains are brecciated into smaller grains which are concentrated in a zone possibly due to post magmatic deformations. The chromite grains contain silicate inclusions, which are also altered to serpentine.

Dunite pods

Dunite pods occur as small elliptical to spheroidal bodies ranging in size from 15 to 60 cm within the mantle tectonite unit. The pods are brownish to buff coloured spherical bodies showing evidence of exfoliation. Dunite pods contain subhedral grains of olivine (~ 92 vol%) and chromite. Olivine occurs both as cumulus and intercumulus phases and is serpentinized, showing relict grains set within a highly serpentinized groundmass of lizardite (Fig. 3d). Chromite occurs as small, rounded, disseminated accessory grains and shows a subsolidus re-equilibration effect where the grains have resorbed boundaries with silicates. The overlapping crystallization of olivine and chromite is demonstrated by the mutual inclusion of chromite and olivine within one another.

Transitional peridotite

The transitional peridotite overlies the tectonite unit with gradational contact and is represented by serpentinized massive harzburgite with different sized pods of dunite.

Harzburgites contain 60-70 vol% olivine, 15-35 vol% orthopyroxene, and 2-3 vol% clinopyroxene, 2-4 vol% chromite. The transitional harzburgites are less altered than mantle tectonites. In altered transitional harzburgites the olivine grains are serpentinized and the pyroxene grains are chloritized, with the presence of relict unaltered grains of pyroxene and minor olivine. Orthopyroxene occurs both as exsolved and unexsolved grains. Both the orthopyroxene and clinopyroxene grains are marginally replaced by olivine. The olivine grains occur in two following different modes: a) as larger relic grains within the serpentinized mass, and b) as small rounded olivine grains, which are fresh and occur mainly along the grain fractures and boundaries of the embayed pyroxene grains. The dissolution of

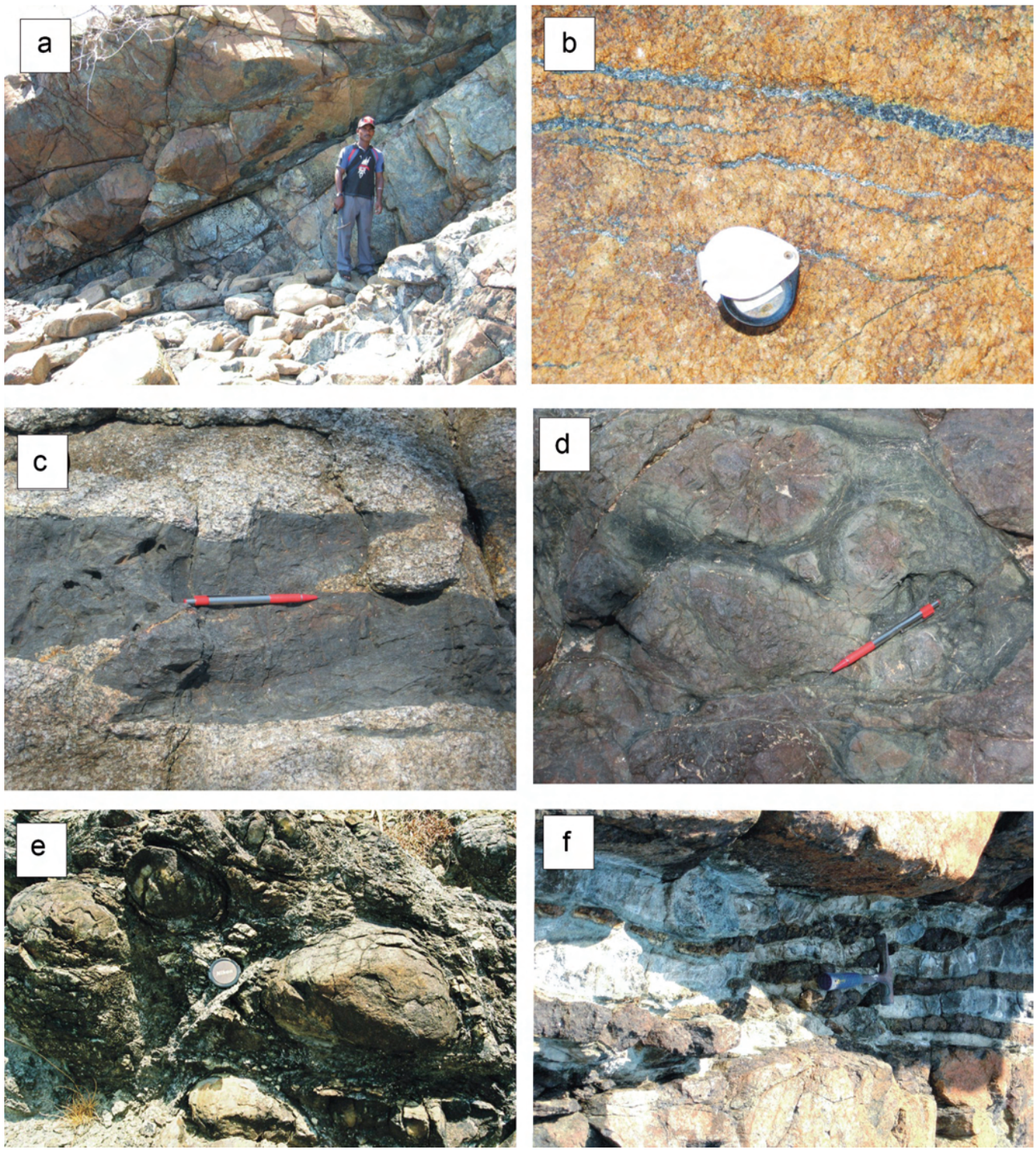

Fig. 2 - a) Layered harzburgite unit showing irregular cracks and joints exposed along the eastern coast of Rutland Island; b) serpentinized dunite with thin (mm to cm scale) stringers of chromite, eastern coast of the island; c) apophyses of altered dolerite in the plagiogranite mass, southeastern coast of the island; d) pillow structure in the red basalt (upper lavas) of the Rutland ophiolite, western coast of the island; e) small dunite pods within the mantle tectonite and, f) sheeted dykes of altered diabase intruded into layered ultramafics, Rutland Island.

clinopyroxene is more common than orthopyroxene, with strongly lobate and irregular clinopyroxene boundaries at olivine front (Fig. 3b). Orthopyroxene grains are also replaced by small olivine neoblasts along the grain boundaries as well as along fractures of large grains (Fig. 3c). The accessory chromite occurs in the form of both irregular and euhedral grains.

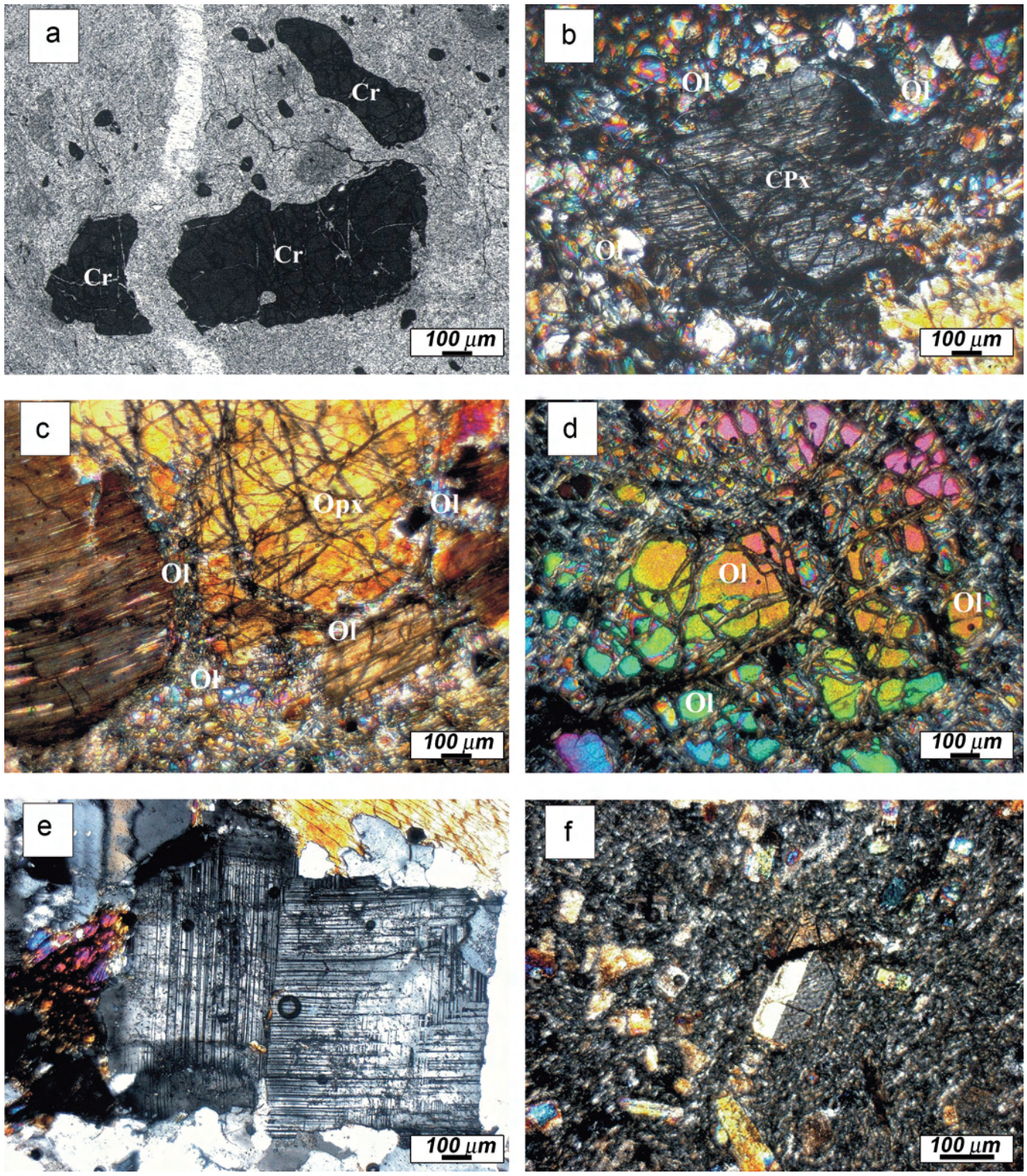

Fig. 3 - a) Fractured chromite grains with irregular boundaries, cut by a thick serpentine vein, within the tectonite unit of the Rutland ophiolite (plane polarized light); b) clinopyroxene grains showing embayed margins replaced by small neoblastic olivine grains through melt-rock interaction (crossed nicols); c) margin of a large orthopyroxene grain surrounded by late small olivine neoblasts (crossed nicols; d) relics of olivine grains in serpentinized dunite (crossed nicols); e) photomicrograph of plagiogranite with subhedral grains of plagioclase and quartz and accessory amphibole showing hypidiomorphic granular texture (crossed nicols), f) porphyritic boninite showing phenocrysts of both orthopyroxene and clinopyroxene in a fine grained matrix containing microlites of albite (crossed nicols).

Layered cumulate

Layered cumulates are composed of ultrabasic and basic rocks. The ultrabasic ones are represented by dunite-harzburgite, whereas the basic cumulate is made of repeated sequences of gabbro and pyroxenite. Harzburgite occurs as a layered and jointed unit, where relict grains of pyroxene are set in the serpentinized mass (Fig. 2a). Dunite is highly altered and contains relict grains of olivine in a serpentinized groundmass. Stringers and disseminations of mm- to cm-scale chromitite bands occur within the dunite (Fig. 2b). Layering in the basic cumulates is defined by alternate pyroxene and plagioclase-rich bands. The gabbro compositionally grades from olivine gabbro to gabbro. Clinopyroxene and plagioclase phases show overlapping crystallization. Plagioclase is often saussuritized and pyroxene is uralitized and chloritized.

Massive intrusives

This unit intrudes into the cumulate and is represented by closely intermingled homogenous gabbro, diorite and plagiogranite.

The homogenous gabbro is a very coarse-grained pegmatoidal rock containing prismatic crystals of primary amphibole as hornblende and laths of plagioclase feldspar. Plagioclase occurs in dual mode, both as unzoned and zoned grains with minor clinopyroxene. It has a restricted field occurrence and is exposed along the southeastern coast of the island.

Diorite is medium to coarse grained and comprises amphibole, plagioclase and biotite. Ilmenite occurs as inclusions both in amphibole and plagioclase.

Plagiogranite occurs as small intrusive bodies within cumulate, with restricted field occurrence and mutual intrusive relationships with diorite. The plagiogranite consists of subhedral grains of plagioclase and quartz with accessory amphibole showing hypidiomorphic granular texture (Fig. 3e). Apophyses of dolerite within plagiogranite unit are also common (Fig. 2c). Parallel to sub parallel dykes of altered dolerite (diabase) within the cumulate sequence occur as sheeted dyke sequence along the south-eastern coastal section of the island (Fig. 2f). In the entire Andaman ophiolite belt the sheeted dyke complex is restricted only to a small area in the Rutland Island.

Extrusive lavas

The extrusive lavas can be classified into two units, lower and upper lavas, based on their lithology and mineralogy.

Lower lavas (rhyodacite - boninite)

Lower lavas are light green, fine grained rocks with restricted field occurrence, along the coastal sections overlying the dyke unit and underlain by the upper lavas.

The mineral composition of the lower lavas varies widely. In some varieties, the rock is fine-grained porphyritic with phenocrysts of oligoclase, sanidine, quartz and minor biotite, set in an aphanitic to glassy, light to intermediate coloured matrix. The fine-grained groundmass constitutes 85% of the rock, whereas oligoclase, the dominant phenocryst constitutes nearly 7% of the rock, followed by quartz (4%), sanidine (3%) and biotite (~ 1%). Mineral composition and modal abundances suggest that it is a rhyodacite. Instead, the other varieties of lower lavas are glassy rocks containing phenocrysts of clinopyroxene, minor orthopyroxene and olivine set in a groundmass of microlitic feldspar, epidote, chlorite, and glass (Fig. 3f).

Boninites in general contain different varieties of pyroxene, minor olivine and chromite as phenocrysts in a glassy matrix, where laths of plagioclase and amphibole are very rare (e.g., Crawford et al., 1989). Therefore the variety of the lower lavas with phenocrysts of pyroxene and olivine set in a glassy matrix suggests a boninitic nature of the melt. The petrological classification for the lower lavas has also been corroborated by major oxide analyses, as described later.

Upper lavas (basalt)

The upper lavas are greenish to reddish-black, massive, brecciated and pillowed volcanics (Fig. 2d) with very limited aerial extent and occur in association with cherts. The extrusive upper lavas are porphyritic with phenocrysts of augite and plagioclase laths set in a glassy to chloritic fine-grained matrix. Fine pyroxene grains are also present in the matrix. Locally the groundmass exhibits subophitic, intersertal or vitrophyric textures. The upper lavas are characterized by glass droplets within the matrix with intricate secondary veins of carbonate, silica and zeolite. Pelagic sediments occurring in association with basalt are represented by greenish to white cryptocrystalline cherts.

DISTRIBUTION OF THE RUTLAND OPHIOLITE SLICES

Detailed field study in the Rutland Island showed dismembered ophiolite bodies, which overlie the finer facies of the Mithakhari Group of sediments with a thrust contact.

Ophiolite slices

On the basis of their mode of occurrence, interrelationship of the ophiolite members with the associated sediments and thrust contacts, four ophiolite slices have been demarcated in the geological map of Rutland Island (Fig. 1c). Three of the four slices, three slices rest over the Mithakhari sediments (Eocene) with a thrust contact and the fourth one is demarcated on the basis of the repetition of the ophiolite sequence as well as the presence of a thrust contact between two ophiolite slices (Fig. 1c, d).

First slice

This is the westernmost ophiolite slice, which is restricted to the southwestern part of the island. It has a gentle dip towards the northwest, which is in contrast with the eastward dip of other slices. This dismembered slice rests over the Mithakhari sediments exposed in the lower contours as a klippe and occupies the higher contours of the hillocks. The north-south striking westerly dipping thrust represents a back- thrust in contrast to the easterly dipping thrusts of other slices. The slice comprises highly serpentinized lherzolite/harzburgite (tectonite), partly serpentinized harzburgite (transitional peridotite), layered dunite-lherzolite-gabbro-pyroxenite (cumulate), dykes of plagiogranite-diorite suite, volcanics of both boninite-rhyodacite and basalt, and minor chert - limestone (pelagic sediments) (Fig 1e) The pelagic sediments occur as disjointed small bodies, which are unmappable at the scale used.

Second slice

This slice has a gentle dip towards the east and is exposed as small isolated patches occupying the higher contour levels in the southeastern part of the island. The second

slice consists dominantly of partly serpentinized harzburgite (transitional peridotite) with minor proportions of layered dunite-lherzolite-gabbro-pyroxenite (cumulate), intrusives of plagiogranite-diorite-non cumulate gabbro suite (exposed at the eastern extremity of the island) and volcanics of both boninite and basalt compositions (Fig. 1e).

Third slice

This is the largest slice having steep dips with N-S strike for kilometers and is exposed as large N-S trending hills/hillocks. The slice rests over the shale facies of the Mithakhari Group along a north-south striking easterly dipping thrust contact. The dip of the thrust plane is steeper compared to those of the first and second slices. The third slice comprises highly serpentinized lherzolite / harzburgite (tectonite) in the lower part and is followed upwards by partly serpentinized harzburgite (transitional peridotite), layered dunite-lherzolite-gabbro-pyroxenite (cumulate) and volcanics of both boninite-rhyodacite and basalt compositions (Fig. 1e).

Fourth slice

This slice, occurring east of the third slice is the easternmost slice. It is distinguished from the third slice on the basis of repetitive ophiolite unit (transitional peridotite overlying cumulate gabbro of the third slice) with a thrust contact between the units. The fourth slice consists dominantly of partly serpentinized harzburgite (transitional peridotite), basalt volcanics, and chert-limestone (pelagic sediments, Fig. 1e).

MINERAL CHEMISTRY (EMPA)

Olivine

The relict olivine grains within the harzburgitic tectonite are forsteritic in composition (Fo_{90-91}) with no variation from core to rim (Table 1). In the transitional peridotite, relics of large olivine grains and small fresh olivines have similar Mg content (Fo_{89-91}) with a slight decrease in Mg content from core to rim and are compositionally similar to those of the tectonites (Table 1).

Pyroxene

The pyroxene grains in harzburgitic tectonites are enstatite (En_{85-89}) (after Morimoto et al., 1988) (Table 2). In the lherzolitic tectonites the orthopyroxene grains occur both as symplectite with spinel (En_{88}) and also as exsolved grains of enstatitic composition. In the lherzolite, clinopyroxene occurs as exsolved grains where a diopsidic ($En_{49}Wo_{48}$) host contains lamellae of enstatite (En_{89}). In the transitional peridotites, orthopyroxene also occurs both as exsolved and unexsolved grains. In the exsolved grains, the host enstatite (En_{89}) shows exsolved lamellae of diopside ($Wo_{47}En_{48}$) (Table 2). The discrete unexsolved grains of orthopyroxene in the transitional harzburgites show high En content (En_{90}). the cumulate gabbro, the cumulus orthopyroxenes are enstatite in composition (En_{77}) (Table 2). The clinopyroxene grains in homogenous gabbro are of augite ($En_{47}Wo_{49}$) composition (Table 2). The pyroxene phenocrysts in boninite are represented by augite ($En_{40-50}Wo_{40-43}$) with no apparent chemical variation from core to rim (Table 2). The pyroxene grains in basalts are essentially augite with a minor variation from core ($En_{51}Wo_{34}$) to rim ($En_{50}Wo_{38}$). The fine grains of pyroxene in the matrix however show lower En content ($En_{48}Wo_{37}$) than the phenocrysts in the basalt (Table 2).

Table 1 - Electron microprobe analysis of olivine from Rutland Ophiolite.

Sample no	10	10	96	96	96	96	88f'	88f'	88f'	94	94
Rock name	Tl	Tl	Th	Th	Th	Th	Trh	Trh	Trh	Trh	Trh
	Core	Rim	Core	Rim	Core	Rim	Core	Rim	Grain	Core	Rim
SiO_2	40.89	40.53	41.27	41.17	41.36	41.17	40.67	40.56	41.63	41.55	41.07
TiO_2	0.00	0.00	0.00	0.00	0.00	0.00	0.02	0.00	0.00	0.00	0.05
Al_2O_3	0.00	0.00	0.00	0.00	0.00	0.00	0.00	0.00	0.00	0.00	0.00
FeO	8.3	9.07	9.17	9.25	9.60	9.25	8.94	11.08	8.40	10.13	10.57
MgO	48.52	47.73	47.8	50.03	50.10	50.03	49.86	48.23	51.54	49.88	49.30
CaO	0.01	0.00	0.00	0.00	0.02	0.00	0.01	0.08	0.01	0.00	0.00
Na_2O	0.04	0.02	0.07	0.02	0.05	0.00	0.04	0.02	0.00	0.02	0.03
K_2O	0.00	0.00	0.02	0.01	0.00	0.00	0.00	0.02	0.00	0.00	0.00
Total	97.76	97.35	98.33	100.45	101.13	100.45	99.54	99.99	101.67	101.58	101.02
Si	1.013	1.011	1.018	0.999	0.999	0.999	0.995	0.997	0.996	1.001	0.997
Al	0.000	0.000	0.000	0.000	0.000	0.000	0.000	0.000	0.000	0.000	0.000
Ti	0.000	0.000	0.000	0.000	0.000	0.000	0.000	0.000	0.000	0.000	0.001
$Fe2^+$	0.172	0.189	0.189	0.188	0.194	0.188	0.183	0.228	0.168	0.204	0.215
Mn	0.003	0.004	0.003	0.000	0.000	0.000	0.004	0.003	0.000	0.002	0.003
Mg	1.792	1.774	1.757	1.810	1.804	1.810	1.818	1.767	1.838	1.792	1.785
Ca	0.000	0.000	0.000	0.000	0.001	0.000	0.000	0.002	0.000	0.000	0.000
Na	0.002	0.001	0.003	0.001	0.002	0.000	0.002	0.001	0.000	0.001	0.001
K	0.000	0.000	0.001	0.000	0.000	0.000	0.000	0.001	0.000	0.000	0.000
Fa	9	10	10	9	10	9	9	11	8	10	11
Fo	91	90	90	91	90	91	91	89	92	90	89

Tl- Tectonized lherzolite, Th- Tectonized harzburgite, Trh- Transitional harzbrgite

Table 2 - Electron microprobe analysis pyroxene of Rutland Ophiolite.

Sample	10	10	10	96	96	94	94	94	88F	R6	91A	5B	17	7	7	7
Rock type	Tl	Tl	Tl	Th	Th	Trh	Trh	Trh	Trh	G	HG	Bn	Bn	B	B	B
Nature of grain	Host	Exsolved lamellae	Symplectite	Host	Unexsolved core	Host	Exsolved lamallae	Discrete	Host	Discrete	Discrete	Discrete	Discrete	Phenocryst Core	Phenocryst Rim	Groundmass
SiO_2	52.51	56.49	53.32	51.83	57.84	56.43	53.92	56.74	56.60	53.37	53.32	53.40	52.12	51.22	51.42	51.20
TiO_2	0.00	0.00	0.00	0.05	0.00	0.00	0.00	0.00	0.00	0.05	0.04	0.07	0.31	0.75	0.74	0.81
Al_2O_3	1.17	2.12	1.80	2.76	1.14	1.78	1.66	1.38	0.91	1.31	2.07	1.24	1.06	2.88	3.56	2.82
FeO	1.87	6.03	5.90	7.07	5.96	6.91	2.38	5.96	6.51	14.21	1.95	5.91	10.64	8.98	7.36	9.18
Cr_2O_3	0.28	0.46	0.72	0.71	0.34	0.26	0.16	0.32	0.17	0.35	0.12	0.19	0.50	0.23	0.15	0.27
MnO	0.13	0.11	0.12	0.09	0.08	0.32	0.44	0.15	0.19	0.00	0.73	0.12	0.00	0.04	0.16	0.07
NiO	0.02	0.01	0.11	0.25	0.20	0.00	0.00	0.15	0.00	0.00	0.00	0.00	0.00	0.00	0.00	0.00
MgO	17.78	33.74	30.22	31.34	31.93	34.54	17.46	31.83	34.83	28.41	17.40	17.82	14.20	17.50	17.44	16.64
CaO	24.56	0.87	1.10	2.35	0.62	0.37	23.85	4.24	0.44	0.64	25.09	19.99	20.98	16.28	18.49	18.10
Na_2O	0.07	0.02	0.04	0.60	0.02	0.06	0.14	0.02	0.02	0.31	0.09	0.08	0.39	0.23	0.26	0.26
K_2O	0.00	0.00	0.01	0.13	0.03	0.02	0.00	0.00	0.02	0.00	0.01	0.00	0.03	0.00	0.02	0.03
Total	98.39	99.85	93.34	97.18	98.16	100.69	100.01	100.79	99.69	98.65	100.82	98.82	100.23	98.11	99.60	99.38
TSi	1.931	1.952	1.985	1.844	2.047	1.932	1.957	1.959	1.954	1.928	1.919	1.973	1.942	1.917	1.888	1.899
TAl	0.051	0.048	0.015	0.116	0.000	0.068	0.043	0.041	0.037	0.056	0.081	0.027	0.047	0.083	0.112	0.101
TFe3	0.000	0.000	0.000	0.000	0.000	0.000	0.000	0.000	0.000	0.000	0.000	0.000	0.000	0.000	0.000	0.000
M1Al	0.000	0.038	0.064	0.000	0.048	0.004	0.028	0.015	0.000	0.000	0.007	0.027	0.000	0.044	0.042	0.023
M1Ti	0.000	0.000	0.000	0.001	0.000	0.000	0.000	0.000	0.000	0.001	0.001	0.002	0.009	0.021	0.020	0.023
M1Fe3	0.000	0.000	0.000	0.000	0.000	0.000	0.000	0.019	0.000	0.000	0.000	0.000	0.000	0.000	0.000	0.000
M1Fe2	0.016	0.000	0.000	0.000	0.000	0.000	0.023	0.000	0.000	0.000	0.055	0.000	0.188	0.000	0.000	0.027
M1Cr	0.008	0.013	0.021	0.020	0.010	0.007	0.005	0.009	0.005	0.010	0.003	0.006	0.015	0.007	0.004	0.008
M1Mg	0.975	0.949	0.912	0.972	0.937	0.989	0.945	0.953	0.995	0.989	0.934	0.965	0.789	0.928	0.933	0.920
M1Ni	0.001	0.000	0.003	0.007	0.006	0.000	0.000	0.004	0.000	0.000	0.000	0.000	0.000	0.000	0.000	0.000
M2Mg	0.000	0.789	0.765	0.691	0.748	0.774	0.000	0.685	0.797	0.541	0.000	0.016	0.000	0.048	0.022	0.000
M2Fe2	0.041	0.174	0.184	0.210	0.176	0.198	0.049	0.153	0.188	0.429	0.004	0.183	0.144	0.281	0.226	0.258
M2Mn	0.004	0.003	0.004	0.003	0.002	0.009	0.014	0.004	0.006	0.000	0.022	0.004	0.000	0.001	0.005	0.002
M2Ca	0.968	0.032	0.044	0.090	0.024	0.014	0.927	0.157	0.016	0.025	0.967	0.791	0.838	0.653	0.728	0.719
M2Na	0.005	0.001	0.003	0.041	0.001	0.004	0.010	0.001	0.001	0.022	0.006	0.006	0.028	0.017	0.019	0.019
M2K	0.000	0.000	0.000	0.006	0.001	0.001	0.000	0.000	0.001	0.000	0.000	0.000	0.001	0.000	0.001	0.001
WO	48.288	1.654	2.299	4.559	1.246	0.684	47.369	7.955	0.813	1.249	48.814	40.390	42.779	34.151	38.024	37.340
EN	48.640	89.234	87.878	84.597	89.278	88.874	48.250	83.094	89.523	77.114	47.102	50.098	40.287	51.079	49.902	47.764
FS	3.072	9.112	9.823	10.844	9.476	10.442	4.380	8.951	9.664	21.637	4.084	9.512	16.934	14.770	12.074	14.896

Tl- Tectonized lherzolite,Th- Tectonized harzburgite,Trh- Transitional harzbrgite , G- Gabbro,HG- Homogenous gabbro, Bn- Boninite, B-Basalt

The Al_2O_3 content of the pyroxene grains in the mantle rocks (tectonite and transitional peridotite) ranges between 0.91 and 2.76 wt% which is a lower value than that of the crustal rocks (cumulates and extrusive lavas) (Al_2O_3 = 1.06-3.56 wt%). The Na_2O content of the pyroxenes (0.02 to 0.60 wt%), however, does not show any regular variation from mantle to crustal rocks.

Chromites

Chromites of the both lherzolitic and harzburgitic tectonites are high-Al, low-Cr-chromites with Al content varying from 20 to 28 wt% Al_2O_3 and Cr content varying from 32 to 38 wt% Cr_2O_3 (Table 3). The chromite grains in the transitional peridotite show a narrow range in composition (42-43 wt% Cr_2O_3 and 18-19 wt% Al_2O_3). The chromites of the chromitite pods are high Cr- low-Al type (58 wt% Cr_2O_3 and 11 wt% Al_2O_3) (Table 3).

Plagioclase

The unaltered discrete grains of plagioclase in the layered gabbro are of labradorite-bytownite composition (An_{61-78}), whereas the altered grains at places show anorthitic composition (An_{96-100}). The unzoned plagioclase grains in the homogenous gabbro are more calcic (An_{60-86}) compared to the zoned plagioclase. The zoned plagioclases are sodic at the cores (An_{49}) and more calcic at the rim (An_{60}). The discrete grains of plagioclase in plagiogranite are typically of albite composition (Ab_{99-100}). In the dioritic rocks the discrete grains of plagioclase are of intermediate composition (An_{34-36}). The plagioclase in the groundmass is present as secondary albite (Ab_{93-99}). Fresh to altered plagioclase phenocrysts in basalt are oligoclase to albite in composition ($Ab_{86-92,}$ Ab_{94-97}) (Table 4).

Amphibole

The amphibole inclusions within the harzburgitic tectonite show a narrow range of chemical compositions with MgO = 18.75 to 19.32 wt%, CaO = 11.98 to 12.22 wt%, Na_2O = 2.12 to 2.17 wt%, K_2O = 0.13 to 0.25 wt% (Table 5). The homogenous gabbro also shows a narrow range of chemical composition with MgO = 13.30 to 14.44 wt%, CaO = 11.38 to 11.75 wt%, Na_2O = 2.04 to 2.49 wt%, K_2O = 0.24 to 0.38 wt% (Table 5). The amphiboles in the dolerite however show a wide range in composition with MgO = 5.70 to 16.37 wt%, CaO = 10.35 to 12.47 wt%, Na_2O = 0.59 to 1.26 wt%, K_2O = 0.06 to 0.16 wt% (Table 5). The amphiboles in harzburgitic tectonites ranges between pargasite and edenite (after Leake et al., 1997). The amphibole in homogenous gabbro ranges in composition from pargasite to magnesiohastingsite (Leake et al., 1997). The amphibole in the diorites is magnesiohornblende (Leake et al., 1997) (Table 5).

PETROCHEMISTRY

Major oxides

The ultramafics of the Rutland ophiolite are highly serpentinized with loss on ignition (LOI) varying from 4.7 to 17.8 wt% (Table 6). The oxides are generally recalculated on a volatile-free basis to minimize the element dilution by serpentinization (e.g., Parkinson and Pearce, 1998). However, the oxide values in the present study are not recalculated, because the petrogenesis of the peridotite will be dealt with the concentration and variation of immobile trace elements, such as Sc, V, Ga, Ti, Zr, Nb (e.g., Lee et al., 2003; Niu, 2004).

The homogenous gabbro has higher CaO (12.03 wt%) and lower SiO_2 contents (46.51 wt%) than the cumulate gabbro (CaO = 8.33 wt%, SiO_2 = 52.65 wt%). Total iron content in the homogenous gabbro (9.79 wt%) is lower than that for cumulate gabbro (11.70 wt%) (Table 6).

The lower lava is represented by boninite and rhyodacite. The composition of the boninite is comparable to Type-2 low-Ca boninite (CaO/Al_2O_3 < 0.55, FeO < 7%, SiO_2 < 58%, MgO: 8.03 to 10.39) (Crawford et al., 1989). On the other hand, the rhyodacite member has SiO_2: 74.51wt%, Al_2O_3: 12.71 wt% ad CaO: 0.17 wt%. The upper lava is

Table 3 - Electron microprobe analysis of chromites from Rutland Ophiolite.

Sample No.	10	96	96	96	94	88F1	88F1	69B	36B
Rock	Tl	Th	Th	Th	Trh	Trh	Trh	Trh	C
TiO_2	0.02	0.00	0.08	0.04	0.02	0.00	0.03	0.04	0.18
Al_2O_3	28.19	26.74	27.06	20.04	18.61	18.39	18.11	9.26	11.21
Cr_2O_3	32.35	32.06	32.44	38.27	42.41	43.27	42.83	55.54	58.15
Fe_2O_3	7.39	6.92	7.52	9.26	8.28	0.00	0.00	5.67	0.00
FeO	17.78	21.29	20.76	21.69	19.94	27.21*	27.27*	20.06	14.79*
MnO	0.25	0.00	0.00	0.00	0.17	0.00	0.00	0.30	0.13
MgO	11.56	11.04	9.75	8.32	9.41	9.26	9.02	8.60	13.96
Total	97.54	98.05	97.61	97.62	98.84	70.92	69.99	99.59	83.63
Ti	0.004	0.000	0.015	0.008	0.004	0.000	0.006	0.008	0.035
Al	8.238	7.721	8.031	6.199	5.676	5.629	5.601	2.940	3.432
Cr	6.342	6.210	6.458	7.941	8.678	8.881	8.883	11.829	11.938
Fe^{3+}	1.380	1.276	1.425	1.828	1.612	7.452	7.439	1.150	2.838
Fe^{2+}	3.687	4.362	4.372	4.760	4.316	20.504	20.576	4.518	12.237
Mn	0.053	0.000	0.000	0.000	0.037	0.000	0.000	0.068	-0.103
Mg	4.273	4.032	3.660	3.256	3.631	9.260	9.020	3.454	13.960
$Cr_{\#}$	43.50	44.58	44.57	56.16	60.45	61.21	61.33	80.09	77.67
$Mg_{\#}$	53.68	48.04	45.57	40.61	45.69	35.42	34.74	43.33	88.65
Al2O3-liquid	nd	nd	nd	nd	nd	nd	nd	nd	10.80
(FeO/MgO)melt	nd	nd	nd	nd	nd	nd	nd	nd	0.67

Tl- Tectonized lherzolite,Th- Tectonized harzburgite,Trh- Transitional harzbrgite, C-Chromitite pods

* Iron was calculated as total Fe, nd: not determined

Table 4a - Electron microprobe analyses of plagioclase feldspar of Rutland Ophiolite.

Sample No.	10A	10A	R6	R6	91	91	91	91	91A	91A	88A	88A	88B	88c	88d	88d	118	118	118
Rock name	G	G	G	G	HG	HG	HG	HG	HG	HG	Dl	Dl	Di	Di	Di	Di	PG	PG	PG
									core	rim	grain	grain			core	rim	core	rim	
SiO_2	68.28	66.98	47.94	52.69	52.77	49.68	50.27	45.51	55.16	52.89	62.77	69.84	59.01	58.48	58.23	56.88	68.91	68.34	68.37
TiO_2	0.00	0.04	0.02	0.01	0.06	0.00	0.00	0.00	0.00	0.00	0.02	0.02	0.01	0.00	0.00	0.00	0.00	0.00	0.00
$Al2O_3$	19.66	20.11	33.06	30.43	29.60	31.72	31.34	33.30	28.80	30.19	24.43	20.12	25.35	25.24	26.15	26.42	19.59	19.92	18.94
FeO	0.03	0.05	0.05	0.07	0.07	0.11	0.13	0.25	0.10	0.14	0.20	0.16	0.00	0.13	0.16	0.14	0.06	0.00	0.06
MnO	0.02	0.00	0.08	0.00	0.00	0.00	0.02	0.09	0.02	0.07	0.03	0.09	0.04	0.00	0.00	0.02	0.01	0.00	0.04
MgO	0.00	0.00	0.00	0.00	0.00	0.00	0.00	0.00	0.01	0.00	0.02	0.01	0.00	0.00	0.00	0.02	0.00	0.00	0.01
CaO	0.01	0.86	16.31	12.86	12.39	15.04	14.25	17.67	10.34	12.44	0.60	0.15	7.45	7.30	7.17	7.28	0.00	0.06	0.00
Na_2O	11.46	11.27	2.53	4.59	4.58	2.96	3.48	1.59	5.88	4.60	8.66	11.98	7.55	7.65	7.19	6.78	11.79	11.89	11.95
K_2O	0.02	0.05	0.00	0.02	0.01	0.03	0.02	0.02	0.03	0.02	2.16	0.05	0.06	0.00	0.06	0.61	0.02	0.04	0.01
Total	99.48	99.36	99.99	100.67	99.48	99.54	99.51	98.43	100.34	100.35	98.89	102.42	99.47	98.80	98.96	98.15	100.38	100.25	99.38
cations on	32 O	32 O	32 O	32 O	32 O	32 O	32 O	32 O	32 O	32 O	32 O	32 O	32 O	32 O	32 O	32 O	32 O	32 O	32 O
Si	11.972	11.809	8.796	9.499	9.608	9.108	9.206	8.533	9.908	9.554	11.196	11.931	10.595	10.576	10.496	10.377	11.987	11.916	12.026
Al	4.060	4.175	7.144	6.461	6.347	6.849	6.759	7.353	6.092	6.423	5.132	4.048	5.360	5.376	5.551	5.676	4.013	4.090	3.923
Ti	0.000	0.005	0.003	0.001	0.008	0.000	0.000	0.000	0.000	0.000	0.003	0.003	0.001	0.000	0.000	0.000	0.000	0.000	0.000
Fe^{2+}	0.004	0.007	0.008	0.011	0.011	0.017	0.020	0.039	0.015	0.021	0.030	0.023	0.000	0.020	0.024	0.021	0.009	0.000	0.009
Mn	0.003	0.000	0.012	0.000	0.000	0.000	0.003	0.014	0.003	0.011	0.005	0.013	0.006	0.000	0.000	0.003	0.001	0.000	0.006
Mg	0.000	0.000	0.000	0.000	0.000	0.000	0.000	0.000	0.003	0.000	0.005	0.003	0.000	0.000	0.000	0.005	0.000	0.000	0.003
Ba	0.000	0.000	0.000	0.000	0.000	0.000	0.000	0.000	0.000	0.000	0.000	0.000	0.000	0.000	0.000	0.000	0.000	0.000	0.000
Ca	0.002	0.162	3.206	2.484	2.417	2.954	2.796	3.550	1.990	2.408	0.115	0.027	1.433	1.415	1.385	1.423	0.000	0.011	0.000
Na	3.896	3.853	0.900	1.604	1.617	1.052	1.236	0.578	2.048	1.611	2.995	3.968	2.628	2.683	2.513	2.398	3.977	4.020	4.076
K	0.004	0.011	0.000	0.005	0.002	0.007	0.005	0.005	0.007	0.005	0.492	0.011	0.014	0.000	0.014	0.142	0.004	0.009	0.002
Total	19.941	20.022	20.069	20.065	20.010	19.987	20.025	20.072	20.066	20.033	19.973	20.027	20.037	20.070	19.983	20.045	19.991	20.046	20.045
Ab	99.8	95.7	21.9	39.2	40.1	26.2	30.6	14.0	50.6	40.0	83.1	99.1	64.5	65.5	64.2	60.5	99.9	99.5	100.0
An	0.1	4.0	78.1	60.7	59.9	73.6	69.3	85.9	49.2	59.8	3.2	0.7	35.2	34.5	35.4	35.9	0.0	0.3	0.0
Or	0.1	0.3	0.0	0.1	0.0	0.2	0.1	0.1	0.2	0.1	13.7	0.3	0.3	0.0	0.4	3.6	0.1	0.2	0.0

G- Gabbro,HG- Homogenous gabbro, Dl-Dolerite, Di- Diorite, PG- Plagio granite, B-Basalt, Bn- Boninite

Table 4b - Electron microprobe analyses of plagioclase feldspar of Rutland Ophiolite.

Sample No.	148b	148b	148b	148b	78B	78B	78B	7	7	7	7	5b	5b	46	46	17	17
Rock name	PG	PG	PG	PG	B	B	B	B	B	B	B	Bn	Bn	Bn	Bn	Bn	Bn
			Core	Rim	Pheno-core	Margin	Microlite	pheno	Phenocore	rim	microlite	matrix	Pheno	Phenocryst-Core	Phenocryst-margin		
SiO_2	61.39	56.57	58.02	59.42	66.56	65.26	66.59	63.01	66.13	67.76	67.05	69.40	69.45	67.53	68.87	67.80	65.26
TiO_2	0.24	0.00	0.00	0.01	0.02	0.00	0.07	0.00	0.01	0.00	0.01	0.00	0.00	0.07	0.05	0.02	0.00
$Al2O_3$	24.00	26.18	26.18	24.68	20.30	19.73	20.65	21.71	21.15	20.79	20.14	20.35	20.12	21.24	20.39	20.41	21.26
FeO	0.42	0.09	0.00	0.08	0.34	1.01	0.16	1.27	0.31	0.33	1.04	0.36	0.04	0.43	0.08	0.10	0.39
MnO	0.01	0.00	0.05	0.00	0.00	0.00	0.05	0.01	0.00	0.00	0.02	0.00	0.00	0.03	0.13	0.00	0.03
MgO	0.00	0.01	0.00	0.02	0.45	1.40	0.06	0.40	0.12	0.02	0.30	0.00	0.01	0.15	0.00	0.00	0.12
CaO	5.57	8.06	7.95	6.16	0.70	0.38	0.95	0.94	0.50	0.46	0.36	0.20	0.09	0.63	0.13	0.31	0.42
Na_2O	8.71	7.09	7.55	8.41	11.31	10.95	10.95	9.71	10.48	11.50	11.86	11.52	11.17	10.88	11.61	11.81	10.41
K_2O	0.06	0.06	0.05	0.08	0.08	0.15	0.14	1.52	0.86	0.16	0.07	0.15	0.03	0.61	0.03	0.07	0.92
Total	100.40	98.06	99.80	98.86	99.76	98.88	99.62	98.57	99.56	101.02	100.85	101.98	100.91	101.57	101.29	100.52	98.81
Cations on	32 O	32 O	32 O	32 O	32 O	32 O	32 O	32 O	32 O	32 O	32 O	32 O	32 O	32 O	32 O	32 O	32 O
Si	10.890	10.340	10.416	10.719	11.718	11.637	11.722	11.362	11.669	11.763	11.725	11.898	11.977	11.684	11.883	11.815	11.616
Al	5.014	5.635	5.535	5.243	4.209	4.143	4.281	4.610	4.395	4.250	4.148	4.091	4.069	4.328	4.143	4.189	4.457
Ti	0.032	0.000	0.000	0.001	0.003	0.000	0.009	0.000	0.001	0.000	0.001	0.000	0.000	0.009	0.006	0.003	0.000
Fe^{2+}	0.062	0.014	0.000	0.012	0.050	0.151	0.024	0.192	0.046	0.048	0.152	0.051	0.006	0.062	0.012	0.015	0.058
Mn	0.002	0.000	0.008	0.000	0.000	0.000	0.007	0.002	0.000	0.000	0.003	0.000	0.000	0.004	0.019	0.000	0.005
Mg	0.000	0.003	0.000	0.005	0.118	0.372	0.016	0.108	0.032	0.005	0.078	0.000	0.003	0.039	0.000	0.000	0.032
Ba	0.000	0.000	0.000	0.000	0.000	0.000	0.000	0.000	0.000	0.000	0.000	0.000	0.000	0.000	0.000	0.000	0.000
Ca	1.059	1.578	1.529	1.191	0.132	0.073	0.179	0.182	0.095	0.086	0.067	0.037	0.017	0.117	0.024	0.058	0.080
Na	2.996	2.513	2.628	2.942	3.861	3.786	3.737	3.395	3.586	3.871	4.021	3.912	3.819	3.650	3.884	3.991	3.593
K	0.014	0.014	0.011	0.018	0.018	0.034	0.031	0.350	0.194	0.035	0.016	0.033	0.007	0.135	0.007	0.016	0.209
Total	20.069	20.097	20.127	20.131	20.109	20.196	20.006	20.201	20.018	20.058	20.211	20.022	19.898	20.028	19.978	20.087	20.050
Ab	73.6	61.2	63.1	70.9	96.3	97.3	94.7	86.5	92.5	97.0	98.0	98.2	99.4	93.5	99.2	98.2	92.6
An	26.0	38.4	36.7	28.7	3.3	1.9	4.5	4.6	2.5	2.2	1.6	0.9	0.4	3.0	0.6	1.4	2.1
Or	0.3	0.3	0.3	0.4	0.4	0.9	0.8	8.9	5.0	0.9	0.4	0.8	0.2	3.5	0.2	0.4	5.4

Table 5a - Electron microprobe analyses of amphibole from Rutalnd Ophiolite.

Rock name	Th	Th	Th	Th	HG	HG	HG	HG	HG	HG	HG	HG	HG	HG	HG	HG
Sample no	96	96	96	96	91	91	91	91	91	91	91	91A	91A	91A	91A	91A
Nature of grain	inclusion in cpx	core	rim	border of pyx	core	rim	inclusion inplag (core)	inclusion inplag (rim)	rim	core	rim	core	rim	rim	core	core
SiO_2	45.89	45.74	45.97	46.46	44.20	43.95	42.74	43.23	42.88	41.94	42.72	43.67	44.33	41.84	42.52	44.37
TiO_2	0.03	0.15	0.08	0.11	1.60	1.60	1.81	1.57	1.29	1.84	1.72	1.75	1.49	2.26	2.27	1.75
Al_2O_3	11.77	12.00	11.73	10.93	11.10	11.79	11.94	11.55	11.48	13.39	12.17	11.16	10.93	12.34	12.64	11.85
FeO	4.47	4.30	4.41	4.11	11.71	11.22	12.33	12.27	12.51	12.32	12.22	12.51	11.61	12.88	12.26	12.08
Cr2O3	2.16	1.97	1.80	2.11	0.00	0.05	0.00	0.01	0.00	0.00	0.01	0.00	0.10	0.00	0.00	0.00
MnO	0.08	0.04	0.00	0.05	0.14	0.18	0.22	0.27	0.20	0.13	0.24	0.21	0.17	0.26	0.18	0.19
MgO	18.93	18.95	18.75	19.32	14.44	14.09	13.87	13.81	13.85	13.31	13.41	14.02	14.19	13.30	13.33	14.13
CaO	12.05	12.12	11.98	12.22	11.56	11.65	11.54	11.71	11.38	11.59	11.75	11.45	11.48	11.41	11.45	11.39
Na_2O	2.17	2.14	2.14	2.12	2.11	2.04	2.24	2.14	2.24	2.49	2.41	2.28	2.20	2.41	2.39	2.30
K_2O	0.25	0.20	0.18	0.13	0.27	0.26	0.28	0.26	0.29	0.24	0.26	0.27	0.30	0.38	0.29	0.30
Total	97.80	97.61	97.04	97.56	97.13	96.83	96.97	96.82	96.12	97.25	96.91	97.32	96.80	97.08	97.33	98.36
TSi	6.424	6.406	6.477	6.508	6.436	6.416	6.262	6.344	6.333	6.142	6.289	6.379	6.492	6.163	6.229	6.396
TAl	1.576	1.594	1.523	1.492	1.564	1.584	1.738	1.656	1.667	1.858	1.711	1.621	1.508	1.837	1.771	1.604
TFe3	0.000	0.000	0.000	0.000	0.000	0.000	0.000	0.000	0.000	0.000	0.000	0.000	0.000	0.000	0.000	0.000
TTi	0.000	0.000	0.000	0.000	0.000	0.000	0.000	0.000	0.000	0.000	0.000	0.000	0.000	0.000	0.000	0.000
Sum_T	8.000	8.000	8.000	8.000	8.000	8.000	8.000	8.000	8.000	8.000	8.000	8.000	8.000	8.000	8.000	8.000
CAl	0.365	0.386	0.423	0.311	0.339	0.443	0.322	0.339	0.330	0.451	0.399	0.298	0.377	0.303	0.409	0.407
CCr	0.239	0.218	0.200	0.233	0.000	0.006	0.000	0.001	0.000	0.000	0.001	0.000	0.012	0.000	0.000	0.000
CFe3	0.372	0.370	0.337	0.356	0.438	0.347	0.530	0.481	0.566	0.443	0.349	0.464	0.324	0.485	0.344	0.384
CTi	0.003	0.016	0.008	0.012	0.175	0.176	0.199	0.173	0.143	0.203	0.190	0.192	0.164	0.250	0.250	0.190
CMg	3.951	3.957	3.938	4.034	3.134	3.066	3.029	3.021	3.050	2.906	2.943	3.053	3.098	2.920	2.911	3.036
CFe2	0.066	0.051	0.093	0.051	0.905	0.951	0.906	0.967	0.899	0.990	1.102	0.980	1.016	1.024	1.074	0.971
CMn	0.005	0.002	0.000	0.003	0.009	0.011	0.014	0.017	0.012	0.008	0.015	0.013	0.010	0.016	0.011	0.011
Sum_C	5	5	5	5	5	5	5	5	5	5	5	5	5	5	5	5
BMg	0	0	0	0	0	0	0	0	0	0	0	0	0	0	0	0
BFe2	0.085	0.082	0.090	0.075	0.083	0.072	0.074	0.057	0.081	0.077	0.053	0.084	0.082	0.077	0.084	0.101
BMn	0.005	0.002	0.000	0.003	0.009	0.011	0.014	0.017	0.013	0.008	0.015	0.013	0.011	0.016	0.011	0.012
BCa	1.807	1.819	1.808	1.834	1.803	1.822	1.811	1.841	1.801	1.819	1.853	1.792	1.801	1.801	1.797	1.759
BNa	0.103	0.096	0.102	0.088	0.105	0.095	0.100	0.085	0.106	0.097	0.078	0.111	0.106	0.106	0.108	0.128
Sum_B	2	2	2	2	2	2	2	2	2	2	2	2	2	2	2	2
ACa	0	0	0	0	0	0	0	0	0	0	0	0	0	0	0	0
ANa	0.487	0.485	0.483	0.487	0.491	0.483	0.536	0.524	0.536	0.610	0.610	0.535	0.519	0.582	0.571	0.515
AK	0.045	0.036	0.032	0.023	0.050	0.048	0.052	0.049	0.055	0.045	0.049	0.050	0.056	0.071	0.054	0.055
Sum_A	0.531	0.520	0.515	0.511	0.541	0.531	0.588	0.573	0.590	0.655	0.659	0.585	0.575	0.654	0.625	0.570
Sum_cat	15.531	15.520	15.515	15.511	15.541	15.531	15.588	15.573	15.590	15.655	15.659	15.585	15.575	15.654	15.625	15.570
Sum_oxy	22.917	22.918	22.934	22.927	23.000	23.000	23.000	23.000	23.000	23.000	23.000	23.000	23.000	23.000	23.000	23.004

Th- Tectonized harzburgite, HG- Homogenous gabbro, Dl- Dolerite

Table 5b - Electron microprobe analyses of amphibole from Rutalnd Ophiolite.

Rock name	HG	Dl	Dl	Dl	Dl	Dl
Sample no	91A	88A	88A	148B	148B	148B
Nature of grain	rim	rim	grain	grain	inclusion feldspar	rim
SiO_2	44.26	50.84	49.15	49.84	50.34	50.86
TiO_2	1.44	0.23	0.31	0.51	0.41	0.52
Al_2O_3	11.62	0.92	4.62	5.00	4.46	4.61
FeO	11.59	24.67	15.19	13.53	14.53	12.49
Cr2O3	0.00	0.00	0.02	0.04	0.00	0.00
MnO	0.20	0.30	0.30	0.39	0.26	0,27
MgO	13.99	5.70	11.08	15.92	15.13	16.37
CaO	11.29	11.54	12.47	11.25	10.35	11.40
Na_2O	2.22	0.65	1.26	0.67	0.59	0.62
K_2O	0.26	0.06	0.16	0.14	0.13	0.10
Total	96.87	94.91	94.56	97.29	96.20	97.24
TSi	6.465	8.119	7.563	7.149	7.307	7.272
TAl	1.535	0.000	0.437	0.809	0.671	0.716
TFe3	0.000	0.000	0.000	0.042	0.022	0.013
TTi	0.000	0.000	0.000	0.000	0.000	0.000
Sum_T	8.000	8.119	8.000	8.000	8.000	8.000
CAl	0.464	0.173	0.400	0.035	0.091	0.060
CCr	0.000	0.000	0.002	0.005	0.000	0.000
CFe3	0.353	0.000	0.000	0.777	0.735	0.636
CTi	0.158	0.028	0.036	0.055	0.045	0.056
CMg	3.046	1.357	2.542	3.404	3.274	3.489
CFe2	0.966	3.295	1.955	0.700	0.839	0.743
CMn	0.012	0.041	0.039	0.023	0.016	0.016
Sum_C	5	5	5	5	5	5
BMg	0	0	0	0	0	0
BFe2	0.097	0.000	0.000	0.103	0.168	0.102
BMn	0.012	0.000	0.000	0.024	0.016	0.016
BCa	1.767	1.867	2.000	1.729	1.610	1.746
BNa	0.124	0.133	0.000	0.092	0.082	0.085
Sum_B	2.000	2.000	2.000	1.948	1.875	1.950
ACa	0	0	0.03	0	0	0
ANa	0.505	0.069	0.376	0.094	0.084	0.087
AK	0.048	0.012	0.031	0.026	0.024	0.018
Sum_A	0.553	0.081	0.437	0.120	0.108	0.105
Sum_cat	15.553	15.200	15.437	15.068	14.984	15.055
Sum_oxy	23.014	23.326	23.252	23.000	23.000	23.000

HG- Homogenous gabbro, Dl- Dolerite

tholeiitic basalt with SiO_2: 42.21-50.28 wt%, MgO: 5.06-6.30 wt%, Al_2O_3 10.92-14.36 wt%, CaO: 6.44-15.79 wt%, total alkalis (Na_2O+K_2O): 3.28 to- 5.44 wt% (Table 6).

Trace elements

The trace element distribution pattern of the homogenous gabbro and diorite shows strong enrichment in Rb and Ba and a slight enrichment in Nb whereas Sr shows a wide variation from enrichment to depletion. Few samples however, show depletion in Zr and Y (Fig. 4). Thus the trace element signature suggests that the source rock was enriched in Rb, Ba, Nb and depleted in Zr and Y.

Both the lower and upper lavas show enrichment in Rb, Ba, Sr compared to N-MORB. But the basaltic lavas have stronger enrichment in those elements than the boninitic lavas. The upper lavas have Zr and Y compositions comparable to those of N-MORB. The lower lava (boninitic) mainly shows Zr and Y compositions comparable with N-MORB but one sample showing depleted Zr and Y suggests that the source for boninitic lavas was slightly depleted in nature (Fig. 4). The trace element pattern, therefore, shows a modified MORB nature for both the variations of volcanic rocks.

The crystallization products ranging from homogenous gabbro to diorite and extrusives (basalt and boninite) are therefore enriched in Rb, Ba, Nb and depleted in Zr, Y. Thus the trace element behaviour in these rocks indicates that the mantle source rock was already depleted in Zr, Y and enriched in Rb, Ba, Nb during melt generation of the crustal sequence.

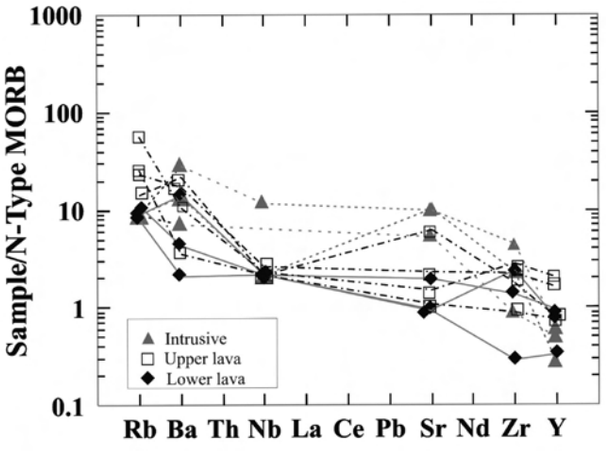

Fig. 4 - Trace element plot showing enrichment of Rb and Ba, slight enrichment in Nb; Sr shows a wide variation from enrichment to depletion, compared to N-MORB (after McDonough and Sun, 1995) from volcanics and intrusives of the Rutland ophiolite. Few samples, however, show depletion in Zr and Y.

DISCUSSION

Melt-rock interaction at a suprasubduction zone (SSZ)

Petrographic features of the transitional peridotites show that both clinopyroxenes and orthopyroxenes were replaced by olivine (Fig. 3b, c). Deformed grains of clinopyroxene are set in an undeformed olivine matrix (Fig. 3b). These textures develop due to melt-rock interaction involving dissolution of pyroxenes and crystallization of olivine (Dick, 1977; Quick, 1981; Kelemen et al., 1990; Pal, 2011). Petrographic observations as well as trace element geochemistry of mantle rocks with high Fo content in olivines could therefore be attributed to the melt-rock interaction, rather than to a high degree of melting (Kelemen et al., 1995; Zhou et al., 1996; 2005).

The widely variable chromite chemistry (42-56% Cr_2O_3 and 9-19% Al_2O_3) can also be attributed to the melt-rock interaction process (e.g., Kelemen et al., 1995; Zhou et al., 1996). As a result of the continuous reaction of melt and rock, the composition of the melt continuously evolved and crystallization paths got modified resulting in precipitation of chromite alone to form chromitite bodies that occur as pods (Zhou et al., 1994).

The chemical plots of the chromites on TiO_2 wt% vs. Al_2O_3 wt% (Fig. 5) diagrams indicate a SSZ setting for the Rutland ophiolite, corroborating with the boninitic affinity of the parental magma.

Melting of the source rock

Tectonite showing lobate grain boundaries of clinopyroxene grains represents a residual phase during partial melting (Menzies, 1973; Parkinson and Pearce, 1998). Very irregular shapes of the Cr-spinel as well as high aluminum content of the chromites within tectonite suggest its residual nature (e.g., Dare et al., 2009). The modal content of clinopyroxene is used to predict the extent of melting (e.g., Niu, 1997).

The presence of ~ 15% modal clinopyroxene represents no melting whereas full consumption of clinopyroxene indicates to ~ 25% melting (Jaques and Green, 1980; Pearce and Parkinson, 1993). The modal 6-13 vol% clinopyroxene within lherzolite of the mantle segment however indicates 5 to 17% melting (e.g., Niu, 1997). But clinopyroxene may persist even for a higher degree of partial melting in case of hydrous melting of peridotite (cf. Parkinson and Pearce, 1998). The clinopyroxene content of the transitional peridotites has not been used as an indicator of melting as the rocks have been influenced by melt-rock interaction.

As fluid activity is common in subduction zone environments; clinopyroxene content cannot be a good indicator for melting. In peridotite, Fo content of olivine is a better indicator for understanding the degree of melting, as olivine-melt equilibria are not changed by fluid activity (Gaetani and Grove, 1998). In olivine, a high Fo content could be related to a high degree of melting but high Fo olivine is also produced during melt-rock interaction (Dick and Fisher, 1984; Zhou et al., 1996; 2005). In the Rutland ophiolite the wide range of Fo content (Fo_{89-92}) of olivine as well as the petrographic features showing replacement of pyroxene by small olivine grains may be attributed to melt-rock interaction rather than to melting. Trace element patterns of mantle rocks usually reflect the influence of both melting and melt-rock interaction processes and it is quite difficult to assess and distinguish the contribution of each of the two processes. Nearly constant trace element concentrations of the mantle rocks of the ophiolite do not give any comprehensive information about the degree of partial melting of the Rutland ophiolite. Under this condition, the Cr# of chromites (Cr# = Cr/Cr + Al), can give significant information about the degree of melting. (e.g., Arai, 1992; Zhou et al.1996; Parkinson and Pearce, 1998). The Cr# vs TiO_2 diagram shows ~ 20% melting for both harzburgite and lherzolite of the tectonite rocks (Fig. 6). The degree of partial melting was also calculated based on Cr# of spinel following the formula F = 10 ln(Cr#) + 24 after Hellebrand et al., (2001) which yields 16 to 18% melting.

These melting estimates represent the total amount of melting (comprising melting in a mid-ocean ridge environment and further melting of the accreted MORB mantle from fluxing by subduction zone fluids). The same diagram (Fig. 6) also shows the influence of melt-rock interaction rather than melting alone in transitional peridotites.

The nature of melting, as for example batch melting or fractional melting can be evaluated by the bivariant relations of MgO with other major oxides (Niu, 1997). At a given MgO value, SiO_2, Al_2O_3 and CaO data are dispersed and do not provide any information on the nature of melting (Fig. 7). The Na_2O and TiO_2 abundances in tectonite are consistent with the calculated residues. The TiO_2 contents of tectonite show closer to batch melting but Na_2O values are closer to fractional melting (Fig. 7). The Al_2O_3, CaO and Na_2O abundances in transitional peridotites are lower than the calculated residues and can be due to addition of olivine (Niu, 1997). Thus the present results do not give any clear idea about the nature of melting.

Nature of magma

To assess the nature of the melts characterizing the evolution of the Rutland ophiolites we have considered the features of the ultramafic rocks, intrusives and extrusives. The chemical compositions of chromite and olivine are used for petrogenesis since they are sensitive petrogenetic indicators (Irvine, 1967; Dick and Bullen, 1984; Barnes, 1986; Auge, 1987; Arai, 1992; Zhou et al., 1996; Melcher

Table 6 - Major oxide (in wt%) and trace element (in ppm) analyses of the different members of the Rutland Ophiolite.

Sample	16B/07	45/07	77/07	18/07	88F/07	94/07	10A/07	91/07	87/07	88C/07	118/07	5A/07	5B/07	46/07	7B/07	78B/07	88A/07
Nature	Tectonite			Transitional			Mafic cumulate	Intrusive			Lower Lava				Upper Lava		
Rock	Harzburgite			Harzburgite			Gabbro	Homogenous gabbro	Dolerite	Diorite	Rhyo-dacite	Boninite			Basalt		
SiO_2	40.10	37.86	37.42	42.79	39.75	41.77	52.65	46.51	48.88	50.55	74.51	52.66	53.28	42.78	42.21	48.59	50.28
TiO_2	0.02	0.03	0.03	0.13	0.01	0.02	1.22	1.29	1.85	1.46	0.40	1.10	0.35	2.46	1.17	1.84	1.33
Al_2O_3	0.26	0.39	0.37	2.33	0.22	0.31	12.54	13.29	12.57	15.49	12.71	13.08	11.08	10.92	12.85	13.20	14.36
Fe_2O_3	6.31	8.22	9.90	4.29	8.56	8.65	4.32	4.93	4.65	2.63	1.85	6.38	4.68	9.36	6.61	11.69	4.35
FeO	0.99	0.36	1.26	4.68	0.27	1.62	7.38	4.86	8.28	3.60	0.54	4.68	5.85	7.92	3.96	1.80	7.74
MnO	0.08	0.17	0.15	0.14	0.12	0.16	0.18	0.12	0.15	0.08	0.03	0.17	0.20	0.27	0.24	0.17	0.18
MgO	38.21	35.57	35.92	37.46	39.58	36.49	5.97	12.12	6.58	7.99	0.67	8.03	10.39	6.30	5.80	5.06	5.79
CaO	0.06	0.07	0.06	2.66	0.54	0.39	8.33	12.03	8.61	9.25	0.17	7.02	6.38	10.57	15.79	8.40	6.44
Na_2O	0.01	0.01	0.01	0.16	0.01	0.05	3.37	1.81	3.79	4.56	6.98	3.20	3.80	2.88	2.53	3.86	5.11
K_2O	0.01	0.01	0.01	0.02	0.01	0.02	0.97	0.20	0.06	0.08	0.12	0.16	0.16	0.40	0.49	1.08	0.33
P_2O_5	0.01	0.01	0.01	0.03	0.01	0.02	0.25	0.03	0.24	1.38	0.08	0.18	0.02	0.22	0.12	0.28	0.30
LOI	14.87	17.75	16.90	4.66	12.17	11.23	1.42	1.56	3.86	1.57	1.41	3.03	2.68	4.91	7.30	3.83	2.14
Total	100.93	100.45	102.04	99.35	101.25	100.73	98.60	98.75	99.52	98.64	99.47	99.69	98.87	98.99	99.07	99.80	98.35
Ba	20	20	20	20	20	20	84	45	84	177	90	27	13	110	22	66	137
Rb	5	5	5	5	5	5	11	5	5	5	5	6	4	13	14	31	8
Sr	5	5	5	22	11	5	515	4737	240	891	85	177	84	205	98	134	566
Y	5	5	5	5	5	5	16	14	35	17	21	26	9	44	21	57	22
Zr	8	9	7	17	9	10	85	64	109	330	176	102	22	167	66	210	130
Nb	5	5	5	5	5	5	5	0	4	27	5	5	5	6	5	5	5
Ga	5	5	5	5	5	5	17	16	17	20	12	17	13	17	18	17	17
Ni	2307	3960	3109	2078	2261	6501	34	100	32	106	5	25	70	36	117	162	17
V	49	57	104	103	50	43	352	449	489	176	30	245	302	403	292	318	544
Cr	2520	2486	2655	2300	2628	1619	50	54	32	99	5	60	397	34	418	109	27
Sc	5	5	5	16	5	5	28	50	29	18	5	32	42	31	24	32	37
Co	99	109	117	108	116	111	28	54	38	38	39	41	42	43	56	26	31

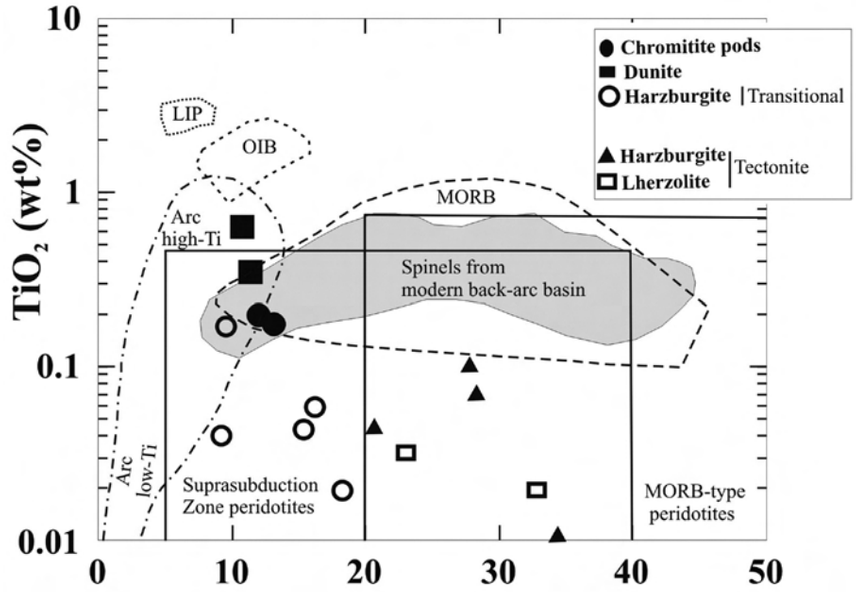

Fig. 5 - Chemical plot of TiO_2 (wt%) vs Al_2O_3 (wt%) showing overlapping fields of MOR and SSZ basalts for the tectonites, whereas the layered peridotites and chromitite pods plot in the SSZ field, Rutland ophiolite.

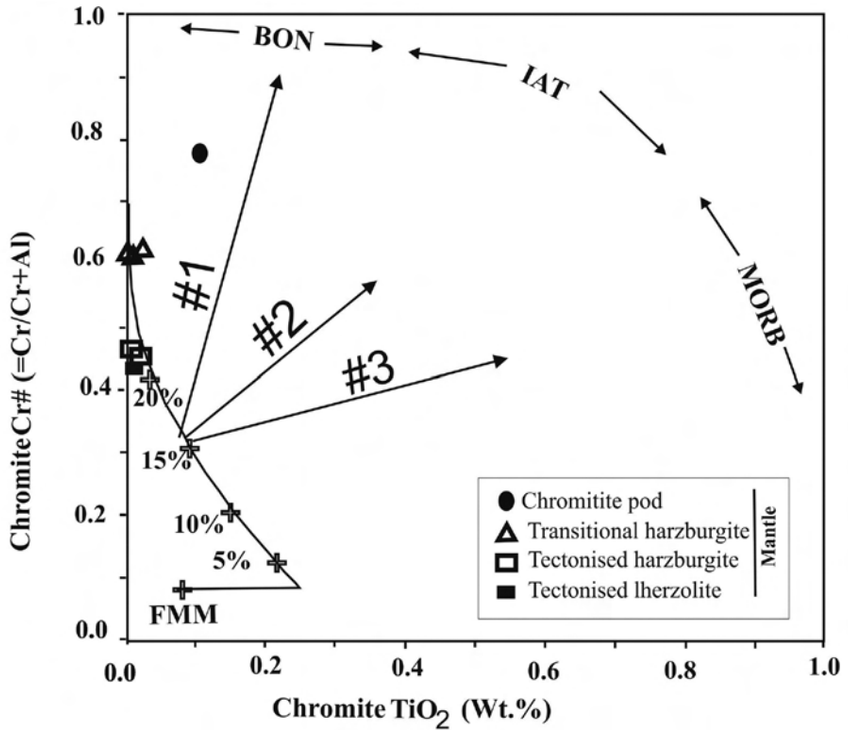

Fig. 6 - Plot of Cr# vs. TiO_2 (wt%) for chromite (Pearce et al., 2000) showing the degree of melting of mantle rocks (curve labelled 5%, 10%, 15%, 20%) and the reaction trends with boninite melts (#1), island arc tholeiite melts (#2) and MORB melts (#3). The Rutland mantle lherzolite and harzburgite are consistent with their residual nature after ~ 20% melting of a fertile MORB mantle (FMM) source. The transitional peridotite shows influence of melt-rock interaction rather than melting alone. Chromites in the chromitite pods have compositions corresponding to melt-rock interaction with bonitic (BON) melts.

et al., 1997; Bedard, 1999). Euhedral chromites in chromitite pods/stringers and in cumulates crystallize from a reacting melt, whereas anhedral chromites are indicative of the residual nature of the mantle lherzolite/harzburgite (e.g., Dare et al., 2009). As the residual rocks (mantle tectonites) of the Rutland ophiolite show anhedral chromites, we have used chromite compositions for these rocks to determine the degree of melting. The euhedral chromites observed in chromitite pods have been used to assess the nature of melt as they represent liquidus chromites. The transitional peridotites of the Rutland Island are characterized by high Mg-olivine (Fo_{89-91}) and high Mg-orthopyroxene (En_{89-90}). The chromitite pods show high Cr-chromites (Cr# 77.67). Orthopyroxenes show very low contents of calcium [$X_{Ca}(M_2)$ = 0.01 to 0.04 a.p.f.u] and aluminium (Al_2O_3 = 0.91 to 2.76 wt%). This assemblage is typical of boninitic melts in supra subduction zone (SSZ) environments (Crawford et al., 1989). The Al_2O_3 content of the parental melt of the chromitite pods is determined as 10.80 wt% (Table 3) following the equation of Maurel and Maurel (1982) cited in Auge (1987). This value suggests a boninitic parental melt composition (Robinson et al., 1983; Auge, 1987). Boninitic parentage has also been reported earlier by Ghosh et al. (2009). The $(FeO/MgO)_{melt}$ value for

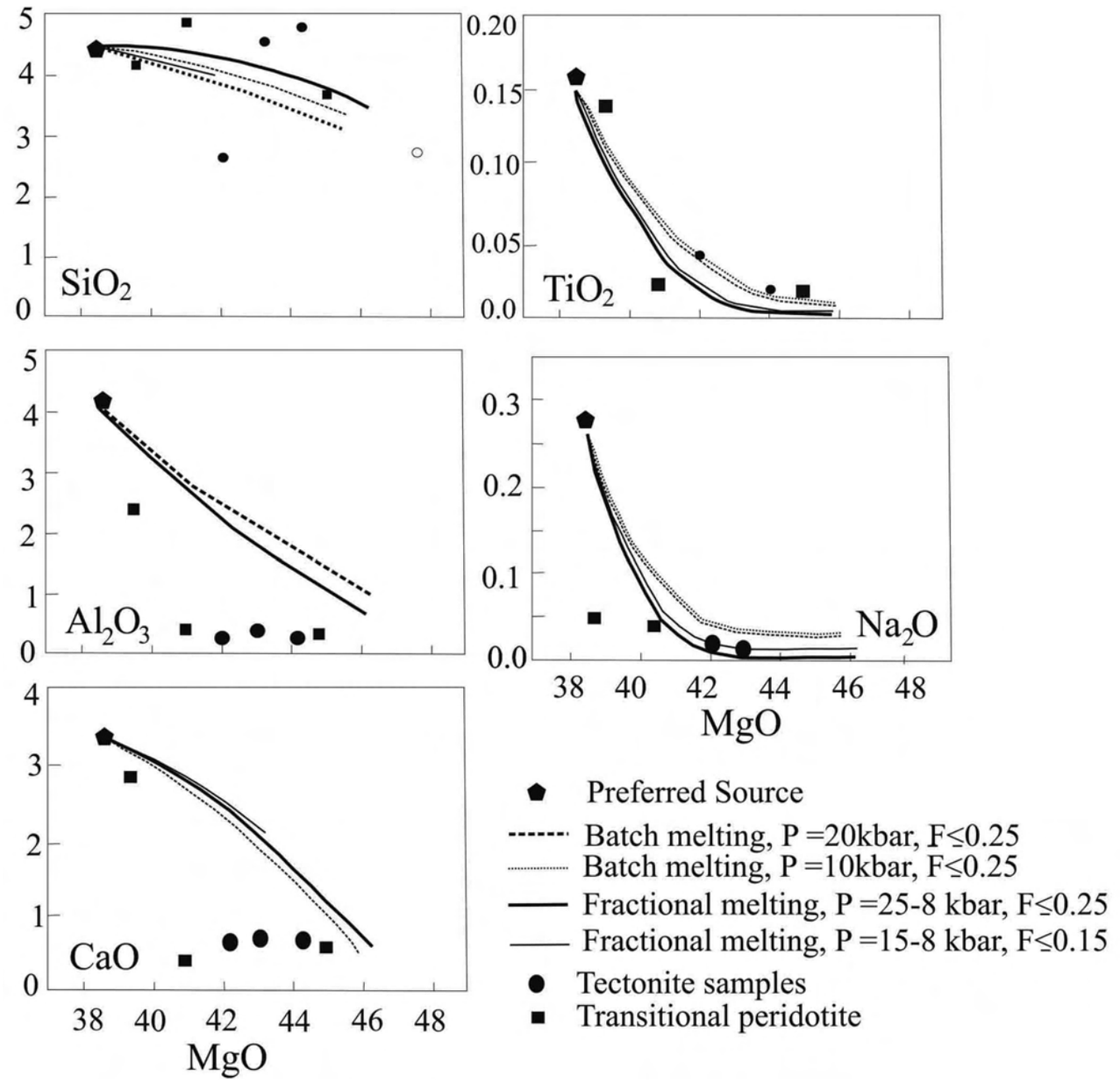

Fig. 7 - Variation diagram of MgO with reconstructed bulk analyses of major oxides (SiO_2, TiO_2, Al_2O_3, CaO and Na_2O) (after Niu, 1997) of tectonite and transitional peridotite showing that SiO_2, Al_2O_3 and CaO against MgO values are dispersed and do not provide clear information about the nature of melting. The TiO_2 contents of tectonite, however, suggest batch melting, whereas the Na_2O values point toward fractional melting.

liquidus chromites, estimated using the empirical formula by Maurel (1984) cited in Auge (1987) is 0.67 which also supports a boninitic source. The Cr# vs TiO_2 relation also indicate a boninitic source of the chromitite pods (Fig 6).

During adiabatic uprise of the mantle the boninitic parental melt could have escaped from diapirs into a big magma chamber to form cumulates (e.g., Gass, 1990). During the late phase of crystallization enrichment of water in the magma chamber yielded primary amphibole in homogenous gabbro (e.g., Falloon and Green, 1987; Hebert and Laurent, 1990). Sometimes MORB-type melt is generated in SSZ environment (Morishita et al., 2010) and MORB melt migration along open fractures can produce such gabbro dykes (e.g., Piccardo et al., 2007 and references therein). The plagiogranite-diorite suite of rocks enriched in Rb, Ba, Nb and depleted in Zr and Y were possibly derived from mafic to intermediate magmas at higher levels (Kistler and Peterman, 1973; Jafri et al., 1995).

The boninitic lower lava is the direct evidence of the boninitic parentage. Chromite phases in lavas are sometimes also used as indicators for their composition (Morishita et al., 2010; 2011). But chromite phases are absent in the lower lava of the Rutland ophiolite. The lower lava (boninitic) shows depletion in Zr and Y compared to N-MORB, suggesting that the source for the lower (boninitic) lava was slightly depleted. Despite the high SiO_2 content in the boninites, depletion of Zr and Y could not result from fractional crystallization of any phases observed in these rocks. Therefore, the trace element data indicate that the source rock for boninite was depleted.

The Zr and Y values for the upper (basaltic) lava are comparable with those of N-MORB. Basaltic rocks show enrichment of Rb, Ba, Sr with respect yo N-MORB and similarity to HFSE and Y with respect to MORB. This implies that the basalts were generated from relatively fertile upper mantle peridotite, which was enriched by a subduction zone component (SZ) (Rogers et al., 1985; Elliot et al., 1997; Turner et al., 1997; Bedard, 1999). However Rb enrichment could also occur during secondary alteration.

Trace element characteristics of the volcanic rocks therefore indicate that at least two phases of the subduction-related magmatism produced the Rutland extrusive sequence. The field features showing occurrence of the basaltic lava above the boninitc lava suggest that the upper basaltic lava was produced at a later stage than the boninitic lower lava.

The enriched trace element pattern of the magmas in the mantle wedge is derived from subducting slab (Rogers et al., 1985; Turner et al., 1997; Bedard, 1999).

During the first stage, the stratigraphically older boninite rocks formed from a relatively depleted source and may have experienced an influx of recycled sediments. During the second stage, with continuing subduction the magmas were generated from a less depleted, possibly MORB-like source forming the stratigraphically younger basalts, which were contaminated principally by fluids from the down-going slab. With continuing subduction, either a change in the dip of the subducting plate or a variation in the sediment imput with time changed the nature of the magmatism from the first to the second phase.

CONCLUSIONS

The Rutland Island is an integral part of the Andaman-Java subduction complex and comprises dismembered tectonic slices of Cretaceous ophiolite interleaved with Eocene sediments. It represents a modern-day subduction complex where the ophiolite slices occur at different structural levels and are emplaced by N-S trending thrust sheets.

The field exposures on Rutland Island show that the majority of thrusts have N-S to NNE-SSW strike with easterly dips and the amount of dip increases from west to east. The tectonic contact of the ophiolite with underlying sediments indicates a thrust-controlled emplacement of these slices (cf. Moores et al., 1984; Platt, 1986; Condie, 1989).

The ophiolite stratigraphy of Rutland Island exposes both the mantle and crustal sections. The mantle tectonite in the form of highly serpentinized lherzolite and harzburgite unit contains spheroidal chromitite pods of high-Cr - low-Al type chromites. The trace element budget and chromite chemistry indicate low to moderate percentages of melting of the source mantle. The residual character of the tectonite is reflected by irregular/embayed grain margins of pyroxene, chromites and high-Al, low-Cr-composition of chromites. Replacement of orthopyroxene and diopsidic clinopyroxene by forsteritic olivine in transitional peridotites suggests melt-rock interaction for the Rutland ophiolite in a SSZ setting. The boninitic parental melt of the ophiolite as estimated from the chromite chemistry is also evidenced by the presence of boninitic extrusives. The crust-mantle behaviour and the evolution of the Rutland ophiolite in a suprasubduction zone setting would be useful to the understanding of the petro-tectonic elements of other parts of the Java - Andaman subduction complex.

ACKNOWLEDGEMENTS

The authors are thankful to Dr. A. Roy, erstwhile Dy. Director General, Eastern Region, Geological Survey of India (GSI) for his administrative help and technical discussions. We express our gratitude to the Director, Petrology Division, ER and the Director, Project Andaman and Nicobar for their support. Assistances from Shri S. Shome of SEM Laboratory, Sri B. Chattopadhyay, Dr. S. Sengupta and Sri. S. Nandy of EPMA Laboratory, GSI, Kolkata are thankfully acknowledged. The authors are thankful to Alberto Zanetti and to an anonymous reviewer for their detailed and critical review of the manuscript. Their comments, suggestions and recommendations significantly improved the paper.

REFERENCES

Arai S., 1992. Chemistry of chromian spinel in volcanic rocks as a potential guide to magma chemistry. Mineral. Mag., 56: 173-184.

Auge T., 1987. Chromite deposits in the northern Oman Ophiolite, mineralogical constraints. Mineral. Dep., *22*: 1-10.

Barnes S.J., 1986. The distribution of chromium among orthopyroxene, spinel and silicate liquid at atmosphere pressure. Geochim. Cosmochim. Acta, 50: 1889-1909.

Bedard J.H., 1999. Petrogenesis of boninites from the Betts Cove Ophiolite, Newfoundland, Canada: identification of subducted source components. J. Petrol., 40: 1853-1889.

Chakraborty P.P., Pal T., Dutta Gupta T. and Gupta K.S., 1999. Facies pattern and depositional motif in an immature trench-slope basin, Eocene Mithakhari Group, Middle Andaman, India. J. Geol. Soc. India, 53: 271-284.

Condie K.C., 1989. Plate tectonics and crustal evolution (3rd edition). Pergamon Press, 469 pp.

Crawford A.J., Fallon T.J. and Green D.H. 1989. Classification, petrogenesis and tectonic setting of boninites. In: A.J. Crawford (Ed.), Boninites. London, Unwin Hyman, 49 pp.

Curray J.R., Fallon T.J. and Green D.H., 1974. Sedimentary and tectonic processes in the Bengal deep sea fan and geosyncline. In: C.A. Burke and C.L. Drake (Eds.), The geology of continental margins. Springer Verlag. New York, p. 617-627.

Dare S.A.S., Pearce J.A., McDonald I. and Styles M.T., 2009. Tectonic discrimination of peridotites using fO_2-Cr# and Ga-Ti-Fe^{III} systematics in chrome-spinel. Chem. Geol., 261: 199-216.

Dick H.J.B., 1977. Evidence of partial melting in the Josepiphine peridotite. In: H.J.B. Dick (Ed.), Magma genesis. Oregon Dept. Geol. Mineral Industries Bull., 86: 59-62.

Dick H.J.B. and Bullen T., 1984. Chromian spinel as petrogenetic indicator in abyssal and alpine-type peridotites and spatially associated lavas. Contrib. Mineral. Petrol., 86: 54-76.

Dick H.J.B. and Fisher R.L. 1984. Mineralogic studies of the residues of mantle melting: abyssal and alpine-type peridotites. In: J. Kornprobst (Ed), Kimberlites II: The mantle and crust mantle relationship. Elsevier, Amsterdam, p. 295-303.

Elliot T., Plank T., Zindler A., White W. and Bourdon B., 1997. Element transport from slab to volcanic front at the Mariana arc. J. Geophys. Res., 102: 14491-15019.

Falloon T.J. and Green D.H., 1987. Glass inclusions in magnesian olivine phenocrysts from Tonga: evidence for highly refractory parental magmas in the Tongan arc. Earth Planet. Sci. Lett., 81: 95-103.

Gaetani G.A. and Grove T.L., 1998. The influence of water on melting of mantle peridotite. Contrib. Mineral. Petrol., 131: 323-346.

Gass I.G., 1990. Ophiolites and oceanic lithospheres. In: J. Malpas, E.M. Moores, Panayiotou and C. Xenophontos (Eds.), Proceed. Symp. 'Troodos 1987'. Geol. Survey, Cyprus., p. 7-33.

Ghosh B., Pal T., Bhattacharya A. and Das D., 2009. Petrogenetic implications of ophiolitic chromite from Rutland Island, Andaman - a boninitic parentage in supra-subduction setting. Miner. Petrol., 96: 59-70.

Hebert R. and Laurent R., 1990. Mineral chemistry of the plutonic section of the Troodos ophiolite: new constraints for genesis of arc related ophiolites. In: J. Malpas, E.M. Moores, A. Panayiotou and C. Xenophontos (Eds.), Proceed. Symp. "Troodos 1987'', Geol. Survey Cyprus, 733 pp.

Hellebrand E., Snow J.E., Dick H.J.B. and Hofmann A.W., 2001. Coupled major and trace elements as indicators of the extent of melting in mid-ocean-ridge peridotites. Nature, 410: 677-681.

Irvine T.N., 1967. Chromian spinel as a petrogenetic indicator. Part II. Petrologic applications. Can. J. Earth Sci., 4: 71-103.

Jafri S.H., Balaram V. and Rames S.L., 1990. Geochemistry of Andaman-Nicobar Island basalts: a case for a possible plume origin. J. Volcan. Geotherm. Res., 44: 339-347.

Jafri S.H., Charan S.N. and Govil P.K., 1995. Plagiogranite from the Andaman Ophiolite belt, Bay of Bengal, India. J. Geol. Soc. London, 152: 681-687.

Jaques A.L. and Green D.H., 1980. Anhydrous melting of peridotite at 0-15 kb pressure and the genesis of tholeiitic basalts. Contrib. Mineral. Petrol., 73: 287-310.

Karig D.E., Suparka S., Moore G.F. and Hehanussa P.E., 1979. Structure and Cenozoic evolution of the Sunda arc in the Central Sumatra Region. In: J.S. Watkins, L. Montadert, and P.W. Dickinson (Eds.), Geological and geophysical investigations of continental margins. Memoir AAPG., 29: 223-237.

Kelemen P.B., Joyce D.M., Webster J.D. and Holloway J.R., 1990. Reaction between ultramafic rock and fractionated rock and fractionating basaltic magma II. Experimental investigation of reaction between olivine tholeiite and harzburgite at 1050-1150ºC and 5 kbar. J. Petrol., 31: 99-134.

Kelemen P.B., Whitehead J.A., Aharonov E. and Jordahl K.A., 1995. Experiments on flow focussing in soluble porous media, with applications to melt extraction from the mantle. J. Geophys. Res., 100: 475-496.

Kistler R.W. and Peterman Z.E., 1973. Variations in Sr, Rb, K, Na and initial $^{87}Sr/^{86}Sr$ in Mesozoic granitic rocks and intruded wall rocks in Central California. Geol. Soc. Am. Bull., 84: 3489-3512.

Leake B.E., Woolley A.R., Arps C.E.S., Birch W.D., Gilbert M.C., Grice J.D., Hawthorne F.C., Kato A., Kisch H.J., Krivovichev V.G., Linthout K., Laird J., Mandarino J.A., Maresch W.V., Nickel E.H., Rock N.M.S., Schumacher J.C., Smith D.C., Stephenson N.C.N., Ungaretti L., Whittaker E.J.W. and Youzhi G., 1997. Nomenclature of amphiboles: Report of the Subcommittee on Amphiboles of the International Mineralogical Association, Commission on New Minerals and Mineral Names. Am. Mineral., 82: 1019-1037.

Lee C.T.A., Brandon A.D. and Norman M., 2003. Vanadium in peridotites as a proxy for paleo-*f*O2 during partial melting: prospects, limitations and implications. Geochim. Cosmochim. Acta, 67: 3045-3064.

McDonough W.F. and Sun S.S., 1995. Composition of the Earth. Chem. Geol., 120: 223-254.

Mckenzie D.P. and O´Nions R.K., 1991. Partial melt distribution from inversion of rare earth element concentrations. J. Petrol., 32: 1021-1091.

Melcher F., Grum W., Simon G., Thathammer V.T. and Stumpfl E.F., 1997. Petrogenesis of the ophiolitic giant chromite deposits of Kempirsai, Kazakhstan - a case study of solid and fluid inclusion in chromites. J Petrol., 38: 1419-1458.

Menzies M., 1973. Mineralogy and partial melt textures within an ultramafic-mafic body, Greece. Contrib. Mineral. Petrol., 42 (4): 273-285.

Mitchell A.H.G. 1985. Collision-related fore-arc and back-arc evolution of the Northern Sunda Arc. Tectonophysics, 116: 323-334.

Morimoto N., Fabries J., Ferguson A.K., Ginzburg I.V., Ross M., Seifert F.A., Zussman J., Aoki K. and Gottardi G., 1988. Nomenclature of pyroxenes. Report of the Subcommittee on Pyroxenes, Commission on New Minerals and Mineral Names, International Mineralogical Association. Am. Mineral., 73: 1123-1133.

Morishita T., Ozawa K. and Obata M., 2010. A recent trend in sciences on mantle-derived materials, with special emphasis on refertilization, rheology, and ophiolite problems: A report on the Fifth International Conference on orogenic lherzolite. Japan. Mag. Mineral. Petrol. Sci., 39 (3): 85-103.

Morishita T., Tani K., Shukuno H., Harigane Y., Tamura A., Kumagai H. and Hellebrand, 2011. Diversity of melt conduits in the Izu-Bonin-Mariana forearc mantle: Implications for the earliest stage of arc magmatism. Geology, 39 (4): 411-414.

Moores E.M., Robinson P.T., Malpas J. and Xenophontos C., 1984. A model for the origin of the Troodos massif, Cyprus and other Mideast ophiolites. Geology, 12: 500-503.

Mukhopadhyay M., 1988. Gravity anomalies and deep structure of the Andaman Arc. Mar. Geophys. Res., 9: 197-211.

Niu Y., 1997. Mantle melting and melt extraction process beneath ocean ridges: Evidence from abyssal peridotites. J. Petrol., 38 (8): 1047-1074.

Niu Y., 2004. Bulk major and trace element compositions of abyssal peridotites: implications for mantle melting, melt extraction and post melting processes beneath Mid-ocean ridges. J. Petrol., 45: 2423-2458.

Pal T., Chakraborty P.P., Duttagupta T. and Singh C.D., 2003. Geodynamic evolution of an outer arc in convergent margin of active Burma- Java subduction complex, a document from Andaman islands, Bay of Bengal. Geol. Mag., 140: 289-307.

Pal T., 2011. Petrology and geochemistry of the Andaman ophiolite: melt-rock interaction in a suprasubduction-zone setting. J. Geol. Soc., London, 168: 1031-1045.

Parkinson I.J. and Pearce J.A., 1998. Peridotites from the Izu-Bonin-Mariana forearc (ODP Leg 125): evidence for mantle melting and melt - mantle interaction in a supra-subduction zone setting. J. Petrol., 39: 1577-1618.

Pearce J.A., Lippard S.J. and Roberts S., 1984. Characteristics and tectonic significance of supra-subduction zone ophiolites. In: B.P. Kokelaar and M.F. Howells (Eds.), Marginal basin geology. J. Geol. Soc. London Spec. Publ., 16: 77-94.

Pearce J.A. and Parkinson I.J., 1993. Trace element models for mantle melting application to volcanic arc petrogenesis. In: H.M. Prichard, T. Alabaster, N.BW Harris and C.R. Neary (Eds.), Magmatic processes and plate tectonics. J. Geol. Soc. London Spec. Publ., 76: 373-403.

Pearce J.A., Barker P.F., Edwards S.J., Parkinson I.J. and Leat P.T., 2000. Geochemistry and tectonic signifcance of peridotites from the South Sandwich arc-basin system, South Atlantic. Contrib. Mineral. Petrol., 139: 36-53.

Piccardo G.B., Zanetti,A. and Műntener O., 2007. Melt/peridotite interaction in the Southern Lanzo peridotite: Field, textural and geochemical evidence. Lithos, 94: 181-209.

Platt J.P., 1986. Dynamics of orogenic wedges and the uplift of high-pressure metamorphic rocks. Geol. Soc. Am. Bull., 97: 1037-53.

Proenza J., Gervilla F., Melgarejo J.C. and Bodinier J.L., 1999. Al- and Cr- rich chromitites from the Mayari-Baracoa ophiolitic belt (eastern Cuba): consequence of interaction between volatile-rich melts and peridotites in supra-subduction mantle. Econ. Geol., 94: 547-566.

Quick J.E., 1981. The origin and significance of large, tabular dunite bodies in the Trinity peridotite, Northern California. Contrib. Mineral. Petrol., 78: 413-422.

Ray K.K., Sengupta S. and Van den Hui H.J., 1988. Chemical characters of volcanic rocks of Andaman Ophiolite, India. J. Geol. Soc. London, 145: 393-400.

Ray K.K., 1982. A review of the geology of Andaman and Nicobar islands. Geol. Survey India, Miscel. Publ., 42 (2): 110-125.

Rogers N.W., Hawkesworth C.J., Parker R.J. and Marsh J.R., 1985. The geochemistry of potasic lavas from Vulsini, central Italy and implications for mantle enrichment processes beneath the Roman region. Contrib. Mineral. Petrol., 90: 244-257.

Robinson P.T., Melson W.G., O'Hearn T. and Schmincke H.U., 1983. Volcanic glass compositions of the Troodos ophiolite, Cyprus. Geology, 11: 400-404.

Roy D.K., Acharyya S.K., Ray K.K., Lahiri T.C. and Sen M.K., 1988. Nature of occurrence and depositional environment of the oceanic pelagic sediments associated with the ophiolite assemblage, South Andaman Island. Indian Minerals, 42: 31-56.

Stern R.N., Lin P.N. and Smoot N.C., 1989. Submarine arc volcanism in the southern Mariana arc as an ophiolite analogue. Tectonophysics, 168: 151-170.

Suhr G., Hellebrand E., Snow J.E., Seck H.A. and Hofmann A.W., 2003. Significance of large, refractory dunite bodies in the upper mantle of Bay of Islands Ophiolite. Geochem. Geophys. Geosyst., G3 4 Paper No. 2001GC000277.

Taylor R.N., Murton B.,J. and Nesbitt R.W., 1992. Chemical transects across intra-oceanic arcs: implications for the tectonic setting of ophiolites. In: L.M. Parson, B.J. Murton and P. Browning (Eds.), Ophiolites and their modern oceanic analogues. J. Geol. Soc. London Spec. Publ., 60: 117-132.

Turner S., Hawkesworth C., Rogers N., Barlett J., Worthington T., Hergt J., Pearce J. and Smith I., 1997. ^{238}U-^{239}Th disequilibria, magma petrogenesis and flux rates beneath the depleted Tonga-Kermadec island arc. Geochim. Cosmochim. Acta, 61: 4855-4884.

Zanetti A., D'Antonio M., Spadea P., Raffone N., Vannucci R. and Bruguier O., 2006. Petrogenesis of mantle peridotites from the Izu-Bonin-Mariana (IBM) forearc. Ofioliti, 31 (2): 183-200.

Zhou M. F., Robinson P.T. and Bai W.J., 1994. Formation of podiform chromitites by melt/rock interaction in the upper mantle. Mineral. Dep., 29: 98-101.

Zhou M.F., Robinson P.T., Malpas J. and Li Z., 1996. Podiform chromitites in the Luobusa ophiolite (southern Tibet): implications for melt/rock interaction and chromite segregation in the upper mantle. J. Petrol., 37: 3-21

Zhou M.F., Robinson P.T., Malpas J., Edwards S.J. and Qi L., 2005. REE and PGE geochemical constraints on the formation of dunites in the Luobusa Ophiolite, Southern Tibet. J. Petrol., 46: 615-639.

Received, February 13, 2013
Accepted, October 28, 2013

Appendix 1 - Precision and accuracy of the bulk chemical anlaysis of the different rock types (compared with the Standard values) of the Rutland ophiolite.

Sample Name	BR	BR	BR	certified values	Av.	SD	DRN	DRN	DRN	certified values	Av.	SD	JP-1	Certified value	LLD (ppm)
Measurement No	1	2	3				1	2	3						
Rock name	Basalt						Diorite						Ultramafic		
SiO_2 (%)	38.23	38.07	38.14	38.20	38.15	0.08	53.65	53.74	53.62	52.85	53.67	0.06	42.39	41.96	Not calc.
Al_2O_3 (%)	9.91	9.9	9.85	10.20	9.89	0.03	16.76	16.79	16.81	17.52	16.79	0.03	0.62	0.63	11
Fe_2O_3(T)(%)	12.77	12.8	12.78	12.88	12.78	0.02	10.09	10.09	10.07	9.7	10.08	0.01	8.34	8.37	9
MnO (%)	0.18	0.17	0.18	0.20	0.18	0.01	0.22	0.22	0.22	0.22	0.22	0.00	0.12	0.13	6
MgO (%)	13.28	13.52	13.55	13.28	13.45	0.15	4.84	4.85	4.86	4.4	4.85	0.01	44.72	45.07	23
CaO (%)	13.91	13.93	13.86	13.80	13.90	0.04	7.12	7.11	7.12	7.05	7.12	0.01	0.56	0.7	Not calc.
Na_2O (%)	3.15	3.12	3.14	3.05	3.14	0.02	2.94	2.93	2.94	2.99	2.94	0.01	0.021	0.03	35
K_2O (%)	1.5	1.53	1.52	1.40	1.52	0.02	1.84	1.84	1.84	1.7	1.84	0.00	0.0033	<0.01	9
TiO_2 (%)	2.48	2.53	2.52	2.60	2.51	0.03	1.18	1.17	1.17	1.09	1.17	0.01			8
P_2O_5 (%)	1.06	1.03	1.04	1.04	1.04	0.02	0.23	0.23	0.23	0.25	0.23	0.00			3
Ba (ppm)	1031	1022	1066	1050	1039.67	23.25	367	330	364	385	353.67	20.55	17	<20	20
Co (ppm)	55	57	53	52	55.00	2.00	40	37	38	35	38.33	1.53	116	119	3
Cr (ppm)	372	376	378	380	375.33	3.06	26	23	28	40	25.67	2.52	2970	2971	10
Cu (ppm)	75	74	77	72	75.33	1.53	52	55	52	50	53.00	1.73	5.7	8	4
Ga (ppm)	18	16	17	19	17.00	1.00	13	19	19	22	17.00	3.46	0.5	<5	4
Nb (ppm)	109	105	107	98	107.00	2.00	9	12	11	7	10.67	1.53	1.2	<5	1
Ni (ppm)	253	247	249	260	249.67	3.06	16	17	16	15	16.33	0.58	2460	2470	3
Pb (ppm)	6	7	5	5	6.00	1.00	55	54	60	55	56.33	3.21	0.11	<5	5
Rb (ppm)	56	56	54	47	55.33	1.15	77	79	78	73	78.00	1.00			2
Sc (ppm)	26	30	30	25	28.67	2.31	31	37	39	28	35.67	4.16	7.07	5	5
Sr (ppm)	1289	1285	1299	1320	1291.00	7.21	422	426	421	400	423.00	2.65			1
Th (ppm)	10	9	8	11	9.00	1.00	<LLD	<LLD	7	5	7.00		0.18	<4	5
U (ppm)	<5	<5	<5	2.5	<5		5	4	7	1.5	5.33	1.53			5
V (ppm)	233	237	238	235	236.00	2.65	246	245	242	220	244.33	2.08	29	33	10
Y (ppm)	31	29	29	30	29.67	1.15	31	27	31	26	29.67	2.31			1
Zn (ppm)	149	155	150	160	151.33	3.21	113	129	126	145	122.67	8.50	29.5	33	5
Zr (ppm)	268	268	267	260	267.67	0.58	153	158	157	125	156.00	2.65	6.3	8	2

Appendix 2 - Composition of the standard used during EMPA study of the different minerals of Rutland ophiolite.

Element	Standard	Composition
Na-Si	Albite	Na 0.0848, Al 0.1008, K 0.0018, O 0.4887, Si 0.3181, Mg 0.0008, Fe 0.0005
Al	Al_2O_3	Al 0.5293, O 0.4707
Fe	Fe_2O_3	Fe 0.6994, O 0.3006
Mg	Olivine	Mg 0.3040, Si 0.1902,Fe 0.0668, O 0.4390
Ca,P	Apatite	P 0.1832,F 0.0340,Cl 0.0035,Ca 0.3902, O 0.3891
Cr	Cr_2O_3	Cr 0.6842 O 0.2142
Mn,Ti	$MnTiO_3$ (synthetic)	Mn 0.3642,Ti 0.3176, O 0.3182
K	Orthoclase	K 0.1348, Na 0.0031, Al 0.0918, Si 0.3108,Fe 0.0100,O 0.4585
Ba	Barite	Ba 0.5884,S 0.1374,O 0.2743
Ni	NiO	Ni 0.7858, O 0.2142
V	Vanadinite	V 0.1048,Pb 0.7380, Cl 0.0262, O 0.1310